UNIVERSITY OF OSLO
Department of Geosciences
MetOs section

Radiative forcing by changes in surface albedo caused by changes in vegetation

Master thesis in Geosciences Meteorology and oceanography

Maria Malene Kvalevåg

June 30th 2005

Abstract

The human influence on vegetation causes changes in the surface reflective properties. By using MODIS land cover and MODIS surface albedo products, an estimation of radiative forcing due to surface albedo changes caused by vegetation changes is performed. A potential natural vegetation data set is used to compute radiative forcing estimates from pre agricultural times to present. A combination between MODIS blacksky and whitesky albedo and diffuse and direct radiation at ground level makes it possible to improve the accuracy of the present surface albedo. A new self-composed surface albedo data set is calculated for the purpose of not overestimating the radiative forcing in snow covered cropland regions. For that reason, a constraint on the pre agricultural data set is carried out by not allowing any surface albedo values to be lower than 0.081. The best estimate shows a radiative forcing due to the surface albedo change of -0.03 W/m^2, which is weaker than what has been claimed earlier by previous studies. This is mainly because of a more realistic value of cropland, the albedo constraint, and also the intrinsic power of the method consisting of combining two MODIS products.

Contents

Chapter 1

Introduction

Since the beginning of agriculture the vegetation canopy has changed in several parts of the world. The effects on climate due to deforestation, urbanization and increasing areas of cropland are very important factors in the global change debate and are not yet completely understood. Human activities that contribute to climate change include in particular the burning of fossil fuels and deforestation, which both cause emissions of carbon dioxide (CO_2), the main gas responsible for climate change, as well as other greenhouse gases. When natural vegetation, like forests, are replaced by agricultural crops, it increases the surface albedo and also increases the energy available in the atmosphere.

Surface albedo is defined as the amount of sunlight reflected by the Earth's surface back to the atmosphere and is highly dependent on the underlying vegetation. It plays a major role in the surface - atmosphere interaction since it determines the amount of available short wave radiation in the system. Areas covered with forest have low albedo, because they absorb light in the visible part of the electromagnetic spectrum instead of reflecting it as flat ground does, i.e deserts and cropland areas. By comparing the surface albedo from present and pre agricultural time, we can estimate the radiative forcing due to the changes in the vegetation. The result is expected to be a global cooling (Hansen et al., 1998; Betts, 2001; Myhre and Myhre, 2003). A data set which provides historical land cover given by Ramankutty and Foley (1999) has made it possible to calculate the difference in surface albedo and to calculate radiative forcing during this period.

The International Panel of Climate Change (IPCC, 2001) have decided to set the Level of Scientific Understanding of the radiative forcing due to surface albedo change caused by land use to "Very Low", and an annual global mean is estimated to be -0.2 W/m^2 within the uncertainty of 0.2 W/m^2 (Hansen et al., 1998; Betts, 2001). Hansen et al. (1998) estimated a global cooling temperature of 0.14° between the preindustrial time and the present. Betts (2001) concluded that agricultural areas in Eurasia and northern North - America have been going through a local cooling of up to 2° during winter and spring season caused by changes in land use since pre agricultural time. An annual mean cooling in the same areas and time period is reported to

be 0.5° - 1°. Betts (2001) pointed out the importance of including anthropogenic effects in land cover changes in General Circulation models (GCM) simulations to detect climate changes. The radiative forcing in the same study was claimed to be -0.2 W/m^2.

The surface albedo increases when the ground is covered with snow and is dependent on the underlying vegetation (Jin et al., 2002). Several physical parameters influence the snow cover such as snow depth, time since last snow fall, temperature history, wind since last snow fall and snow impurities (Aoki et al., 2003). This makes the calculation of radiative forcing due to surface albedo more complex and is the origin of the high uncertainty recorded.

Myhre and Myhre (2003) calculated in their sensitivity study that the radiative forcing caused by land cover changes depends on the surface albedo data set used. They estimated radiative forcing with three different surface albedo data sets: SARB, Wilson and Henderson-Sellers and Matthews. The data sets differ in the number of land cover classes they include. The radiative forcing in this study varies from -0.02, -0.29 and -0.19 W/m^2, respectively, when using a potential natural vegetation data set given by Ramankutty and Foley (1999). The difference between the forcing estimates is due to the uncertainty values of cropland which range from 0.15 to 0.20. In the study of land cover change by Matthews et al. (2003), they estimated the total change in temperature the past three hundred years as a cooling of 0.09° or 0.17°, depending on the cropland value which was set to be 0.17 and 0.20 respectively, for the two cooling estimates. The main precept in almost all of the papers concerning land use and climate change is the need for more research.

This study will contribute to the subject by calculating the radiative forcing due to surface albedo change caused by vegetation change using higher resolution data sets. The estimates will include satellite retrievals combined with seasonal variability in albedo values. By going through different steps to improve the results, this study will end up with a data set including observational surface albedo data from the MODerate resolution and Imaging Spectroradiometer (MODIS). Then we will use this as an estimate of the present albedo and also to compute a new surface albedo from pre agricultural time. The results will show the strength of the method using MODIS surface albedo data in combination with the MODIS land cover product. Expectantly, this will lead to a better knowledge about the impacts that surface albedo changes caused by vegetation changes have on the global radiation balance, enabling to reduce inherent uncertanties.

Chapter 2

Theory of radiative transfer

2.1 Concept of short wave radiation

Radiation from the sun includes all wavelengths. 40 % of the incoming solar radiation is in the visible (VIS) spectrum (0.4 - 0.7 μm), 10 % is below (< 0.4 μm) and 50 % is beyond the VIS. Since 99 % of all wavelengths from the sun that reach our planet are below 3.8 μm, which is in the infrared (IR) region, radiation from the sun is referred to as shortwave radiation. Quantities for measuring shortwave radiation are flux density (irradiance) or intensity (radiance). To describe the radiative measuring units, I_λ and F_λ, we have to define the concept of the solid angle, Ω. The solid angle is defined as the ratio of an outline area A on a sphere to the square of the radius r, Equation 2.1, and is in unit of steradian (sr).

$$\Omega = \sigma / r^2 \tag{2.1}$$

Accordingly, the differential solid angle is $d\Omega = d\sigma/r^2$ and may be written in polar coordinates as $d\Omega = sin\theta d\theta d\phi$, where θ and ϕ express the zenith and azimuth angles, respectively. The monochromatic irradiance F_λ, is the amount of energy carried by the radiation per second per unit area and is in units of $[\frac{J}{s\ m^2}]$ or $[\frac{W}{m^2}]$. According to the definition, F_λ may be calculated as shown in Equation 2.2.

$$F_\lambda = \int_0^{2\pi} \int_0^{\pi/2} I_\lambda(\theta, \phi) cos\ \theta sin\ \theta\ d\theta d\phi \tag{2.2}$$

By integrating the monochromatic irradiance over the entire electromagnetic spectrum we get the total flux density, $F = \int_0^\infty F_\lambda\ d\lambda$. Monochromatic radiance is the radiant intensity per unit surface area which the energy is being intercepted expressed by the solid angle, Equation 2.3. This also gives us more specific information on the *directional* dependence of the energy flow.

$$I_\lambda = \frac{dE_\lambda}{cos\theta\ d\Omega\ d\lambda\ dt\ dA} \tag{2.3}$$

Consequently the units of radiance is in $[\frac{W}{m^2\ sr}]$.

2.2 Equations of radiative transfer

When a beam of sunlight is transversing a medium, the intensity of this direct radiation will undergo a change caused by absorption and scattering. The result of the changes is called extinction and happens at discrete wavelengths. The extinction is calculated from a geometrical area of a particle and is also referred to as *mass extinction cross section*, k_λ. In radiative transfer we use a term called extinction *coefficient*, $\beta_e = k_\lambda\ \rho$, which is the mass extinction cross section multiplied with the density of the medium ρ, and is in unit of [cm^{-1}].

If we have a simple case of a beam of light coming through a non scattering medium, the beam will be attenuated and this will lead to a reduction in the intensity, δI_λ. The attenuation is only caused by absorption through the media. The total change within the layer at a distance ds, can be summarized in Equation 2.4.

$$\delta I_\lambda = -I_\lambda\ \rho k_\lambda\ \delta s \tag{2.4}$$

If we set the boundary conditions to be an intensity $I_\lambda(0)$ at s= s_0, then the out coming radiation at s = s_1 after transversing the medium is given in the solution of Equation 2.4. Equation 2.5 is called Beers Law and we see that the radiative intensity decreases exponentially through the layer depending on the absorption coefficient k_λ, and the path length which is defined as u = $\int_0^{s_1} \rho$ ds.

$$I_\lambda(s_1) = I_\lambda(0)e^{-k_\lambda u} \tag{2.5}$$

For a more realistic and complex case, we now consider a beam of light coming through a layer in our atmosphere. Both absorption and scattering will influence the radiation. If the beam hits the top-layer without first being scattered, it is called direct solar radiation. On the other hand, if the beam is scattered, we call it diffuse radiation. Since we are considering a plane-parallel atmosphere, the incident light is coming from direction (μ, ϕ) and is scattered out in the direction (μ', ϕ'). μ is defined as *cos* θ, where θ is the angle between the incoming radiation and the normal of incidence, also called zenith angle. ϕ is the angle corresponding to the incoming radiation in the x-plane, also called azimuth angle. The scattering of the unscattered direct sunlight is called single scattering. All other scattering processes are referred to as multiple scattering. The incoming direction of the solar irradiance is (μ_0, ϕ_0) and scatters out again in direction (μ, ϕ). Further we define the *singel-scattering albedo* as the ratio of the scattering coefficient to the extinction coefficient in the form $\tilde{\omega} = \beta_s/\beta_e$. We use the optical thickness $\tau = \int_z^\infty \beta_e dz'$ as the vertical coordinate. Note that τ increases downwards which is convenient in short wave radiation calculations. The phase function P, is a normalized non dimensional parameter and explains the distribution of the multiple and single scattered radiation. We can now describe the fundamental radiative transfer equation.

$$\mu \frac{\delta I(\tau,\mu,\phi)}{\delta\tau} = I(\tau,\mu,\phi) - \frac{\tilde{\omega}}{4\pi}\int_0^{2\pi}\int_{-1}^{1} I(\tau,\mu',\phi')\ P(\mu,\phi;\mu',\phi')\ d\mu' d\phi' - \frac{\tilde{\omega}}{4\pi}\ F_{\odot}\ P(\mu,\phi;\mu_0,\phi_0)e^{-\tau/\mu_0} \quad (2.6)$$

Equation 2.6 may be solved numerically by using discrete ordinates method (DISORT) with a predefined number of streams.

2.3 Short Wave Radiation model

The radiative transfer equation (RTE), Equation 2.6, is solved numerically in a Short wave Radiation Model (SRM) which include the DISORT algorithm made by Stamnes et al. (1988). This is the same model which is used in the study by Myhre and Myhre (2003). The model runs with 8 streams to approximate the radiative transfer system in the atmosphere. The RTE is dependent on both azimuth angle, ϕ, and polar angle, μ. DISORT uses the azimuth averaged version of Equation 2.6. The computations are made by using optical thickness as the vertical coordinate and the polar angle to describe the direction of the radiation. The number of polar angles are the streams that represent the radiation in the whole atmosphere. They always come in pairs (2, 4, 6, etc.) because of an equal representation in the up and down-welling direction. Typical DISORT outputs are net fluxes up and down at the top of the atmosphere (TOA) and albedo at the surface. The resolution is set to approximately 1.9° x 1.9° (T63) and 19 levels in the vertical. The SRM include absorption and scattering by aerosols, scattering by clouds, Rayleigh scattering and absorption of atmospheric gases such as O_3 and H_2O. The meteorological data in the model are from the European Center for Medium-range Weather Forecast and are monthly means.

2.4 Radiative forcing

Calculating the global radiative forcing is a good indicator for analyzing climate changes. The radiative forcing is defined as a perturbation in the radiation balance of the surface-troposphere system (IPCC, 2001). The dynamical properties of the stratospheric system stay unmodified as well as the secondary effect caused by the changes in the troposphere. The climate system responds to the radiative forcing so as to re-establish the energy balance and the calculation of net irradiance is done at the tropopause level after a readjustment of the stratospheric temperature to radiative equilibrium. The Solar constant (R) tells us how much incoming short wave radiation that reaches TOA, and this constant is measured by several satellites to be approximately 1366 W/m^2 but varies between ±2 % due to fluctuations in emissions from the Sun. The radiative forcing (RF in Equation 2.8) can now be calculated as the difference in flux from two special scenarios. For this purpose that is the difference between flux at TOA at present time, F_{pres}, and flux at TOA computed with a data set including potential natural vegetation, F_{potv}. The radiative forcing tells us whether there has been a cooling or a heating of the atmosphere during this time period. The unit of radiative forcing is in W/m^2.

2.4.1 TOA shortwave radiation budget

When dealing with a global short wave radiation budget, the easiest and most comprehendible way to investigate is to calculate net fluxes at TOA. From our definition of radiative forcing, we analyze net fluxes at tropopause level. Myhre and Stordal (2001) tested the difference in evaluating the radiative forcing at the real top of the atmosphere or at the tropopause level with a stratospheric temperature adjustment. For thermal infrared radiation, the forcing was 10 % weaker at tropopause level than at TOA, and for surface albedo this value is expected to be even weaker. The net short wave radiation at TOA, F_{NET}, is calculated by subtracting the up-welling flux from the incoming solar radiation (divided by four since the Earth is a sphere), Equation 2.7. The up- and down-welling fluxes include both diffuse and direct radiation.

$$F_{NET} = \frac{1}{4}R - F^{\uparrow}_{TOA} \tag{2.7}$$

Both F_{pres} and F_{potv} are computed by the model. Equation 2.8 shows how the radiative forcing (RF) is calculated. The solar constant R is claimed to be unchanged during this time period.

$$\begin{aligned} RF &= \frac{1}{4}R - F^{\uparrow}_{TOA_{pres}} - (\frac{1}{4}R - F^{\uparrow}_{TOA_{potv}}) \\ &= -F^{\uparrow}_{TOA_{pres}} + F^{\uparrow}_{TOA_{potv}} \end{aligned} \tag{2.8}$$

For an annual global mean, the quantity RF will have a negative value since an expected albedo increase causes an increasing flux at TOA at present time compared to pre agricultural time. The RF will locally reach positive values due to a surface albedo decrease. This can be caused by either grassland or desert areas with relatively high albedo values which has been forested or converted to cropland. Figure 2.1 shows how the annual global flux at TOA is distributed. The areas where the upwelling flux at TOA reaches its maximum, are either where the cloud cover is high or there is a large aerosol optical depth, as discussed below. In Northern Hemisphere (NH) mid-latitude, both high snow cover and high cloud cover result in an annual irradiance of approximately 80 - 100 W/m^2.

2.5 Diffuse and direct radiation

Both diffuse and direct radiation are present in the Earth's atmosphere. Direct radiation is when the sun light penetrates through the atmosphere without getting attenuated by being absorbed by gases in the atmosphere, scattered by Rayleigh scattering etc. The radiation that is being scattered out of the direct beam is called diffuse radiation. The last term in the equation of radiative transfer, Equation 2.6, explains how the direct solar beam, $F_{\odot}$, is exponential attenuated through layers in the atmosphere. The diffuse radiation is described in the second term of Equation 2.6 and is also called the multiple scattering term. To get the contribution from both the diffuse and direct component, a relative variable S is computed in terms

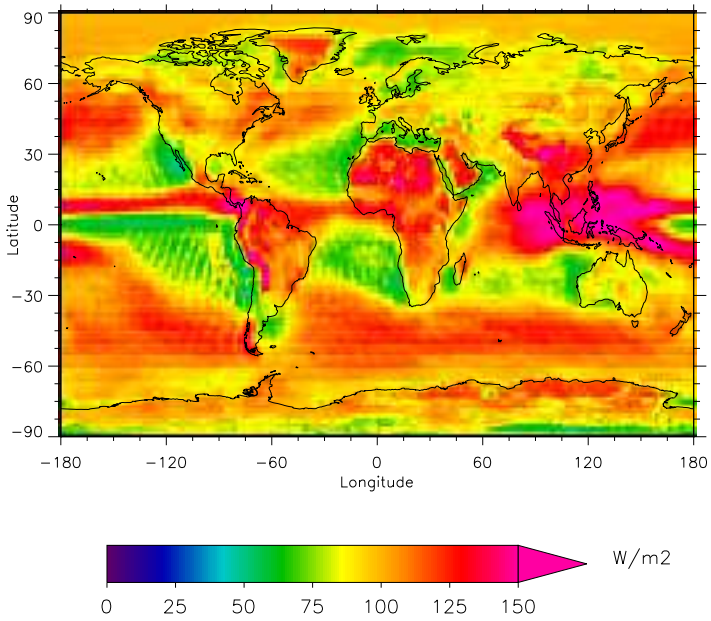

Figure 2.1: Annual mean net flux at TOA

of explaining the ratio between diffuse and total radiation, Equation 2.9. S_{diff} and S_{dir} are the down-coming fluxes, diffuse and direct respectively, at bottom of atmosphere (BOA) in W/m^2.

$$S = \frac{S_{diff}}{(S_{diff} + S_{dir})} \tag{2.9}$$

When S reaches its minimum, S_{min} is equal to only having direct radiation coming through the atmosphere and hit the surface. According to this, S_{max} is then when the incoming solar beam has been scattered or absorbed before it reaches the ground level. In the model, calculating S is an iteration process since it is used in the further computation of the surface albedo (Equation 3.3). The diffuse radiation varies at every step, but the direct radiation stays constant during the process. The annual global mean of diffuse and direct radiation that reaches the Earth's surface is computed by the model after two iterations to be 87.1 W/m^2 and 83.0 W/m^2, respectively. S is sensible to all elements that cause the diffuse radiation to change. Clouds and aerosols will increase the amount of diffuse radiation and hence S will have both a latitudinal and a seasonal variation. The amount of diffuse radiation increases northward from the South Pole and reaches its maximum at equator before it decreases again to wards the North Pole. Figure 2.2 shows this variation for the diffuse radiation and includes the total of possible contributors which are scattering by clouds, absorption by gases, Rayleigh

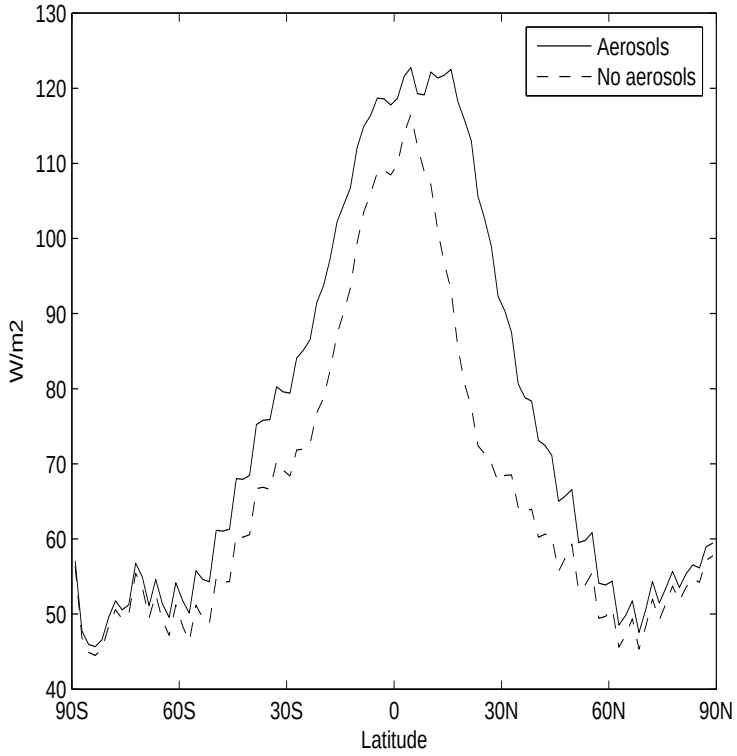

Figure 2.2: Annual zonal mean of total diffuse radiation at BOA with and without aerosols

scattering, and surface albedo reflections. This gives us the total diffuse radiation that reaches the surface. The reason for the maximum flux near equator is the high amount of clouds in the tropical region. Also shown in the figure is the amount of diffuse radiation at BOA without aerosols. The difference between them is highest between 0° - 30°N. This is because the high appearance of mineral dust over the Sahara desert. At mid-latitude, the change in diffuse radiation caused by aerosols is minimal, but still more significant than in the Southern Hemisphere (SH). The continental area is much less in SH which results in only a small increase of aerosol optical thickness caused by sea salt. To analyze the effect of the different absorption and scattering processes on the diffuse and direct radiation, we can compute flux at TOA for a single contributor, as seen in Figure 2.3. Annual global mean flux at TOA is computed by the model to be 101.5 W/m^2. Without clouds, the annual global mean flux at TOA decreases by approximately 50 % and reaches 52.6 W/m^2. The major reason for the zonal pattern of flux at TOA is the present of clouds in the model. There are three peaks in the cloud distribution which are caused by the relative high cloud cover over a longitude band north of Antarctica, the Inter Tropical Convergence Zone (ITCZ), and a medium high cloud cover over mid-latitudes. The surface albedo contributes most to the flux at TOA at higher latitudes because of reflections of snow. We can also see the peak at 10° - 20°N because of high

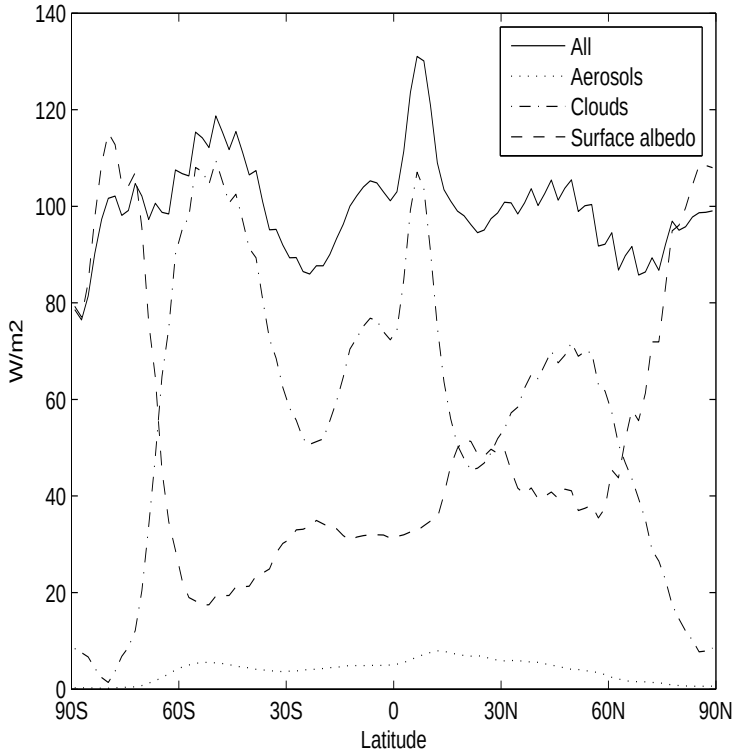

Figure 2.3: Annual zonal mean of flux at TOA with all the single model contributors

reflection over the Sahara. The low reflectance between 30° - 60°S is due to the oceanic area over the Pacific and the South Atlantic. Aerosols contribute less to the total flux at TOA, but we can see the small maximum peak over the Sahara where they increase the diffuse radiation significantly.

2.5.1 Clouds

Clouds cover approximately 60 % of the Earth and their reflective characters are important in the radiative calculations. Radiation through a layer of clouds is dependent on several properties such as cloud droplet size, ice particle shape, droplet distribution and cloud thickness. The most serious problem about satellite retrievals of vegetation canopy is due to cloud cover (Jin et al., 2003). 8 % of the pixels in september are no value data caused by the invisibility of the Earth's surface because of the impenetrably cloudy atmosphere. Cloud cover has a major effect on the amount of diffuse radiation. Figure 2.4 shows the seasonal global distribution of S for an aerosol-free atmosphere based on model computations. The pattern is caused by the distribution of clouds and how their scattering processes affect the diffuse radiation. As S reaches 1 in Figure 2.4, a totally cloud cover is present and it corresponds to pure diffuse radiation at ground level. This is seen in southern latitudes where we have 80 - 90 % cloud cover over 40° - 70°S. The low values of S are found especially over clear sky areas such as the Sahara

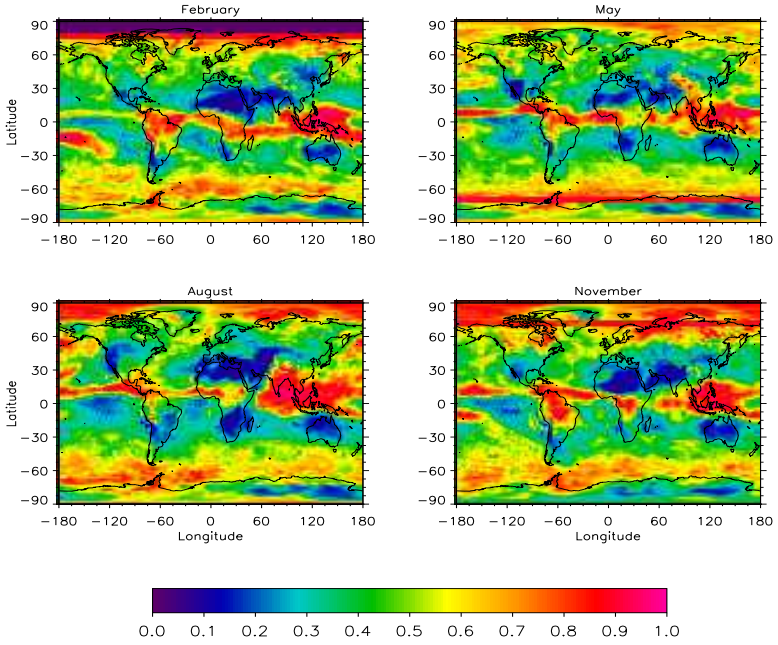

Figure 2.4: The seasonal variation of S without aerosols

and Gobi deserts. The overall seasonal variation is not that large except in mid-latitude areas around 60°N. In that region, cloud covers less then 50 % during local summertime, and exceeds 50 % during NH wintertime and are the major contributor to the high value of S. In all four seasons, S reaches a minimum north and south of the diffuse radiation peak at equator and increases to wards the poles. In August we see the high density of clouds that cover southern parts of Asia which makes S to reach 1. This is related to the bad satellite retrievals during the same period as mentioned above. The ITCZ is easily seen where clouds cover south of equator during November/February, and is moving northward in the NH summer, May/August. Figure 2.4 also shows the fact that the ITCZ is stable over oceanic areas.

2.5.2 Aerosols

The scattering process causes the sun light to be broken into several beams in all directions. When aerosols are included in the model, the occurrence of redirected sunlight rises and produce more diffuse radiation. Aerosols are small particles in the atmosphere and range in size from approximately 10^{-3} - 10μm. They appear naturally as well as anthropogenic both over seas and continental areas, and their concentrations are between 10^{7} - 10^{-6}cm^{-3} depending on location and type. Aerosol optical thickness (AOT) is a measurement of the atmospheric opaqueness. Equation 2.10 defines the total op-

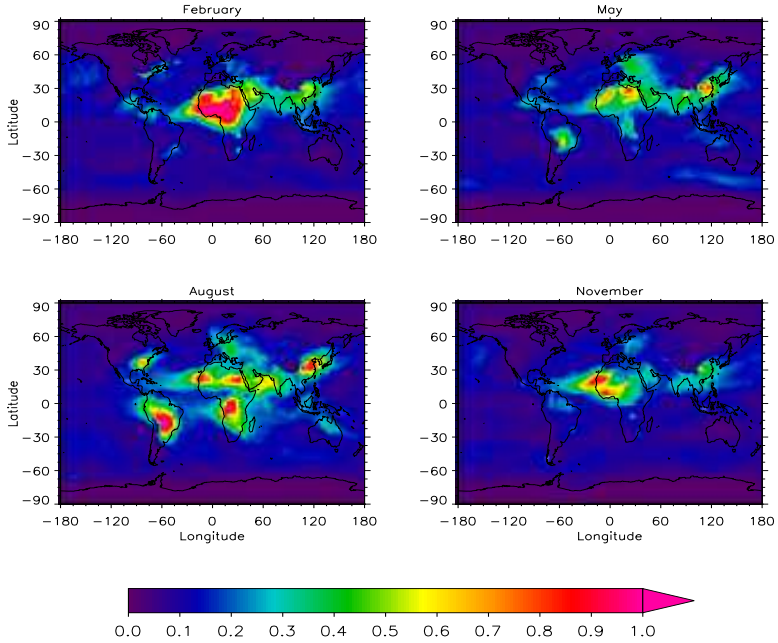

Figure 2.5: The seasonal variation of aerosol optical thickness

tical thickness, τ, by integrating over a vertical path, dz, which the sunbeam penetrates and is weakened by extinction, β_e.

$$\tau = \int_z^\infty \beta_e dz' \tag{2.10}$$

If we only consider the contribution from the aerosols, the aerosol optical thickness, τ_A, is globally distributed as shown in Figure 2.5. Other contributors to the total optical thickness are Rayleigh scattering molecules and absorption of gases in the atmosphere. The five types of aerosols included in the model are mineral dust, sea salt, black carbon (from fossil fuels and biomass burning), organic carbonaceous (from fossil fuels and biomass burning), and sulfate. They are all monthly means based on simulations from a chemistry transport model in a global aerosol intercomparision study (AEROCOM). The location of the different types of aerosols vary, and Figure 2.5 shows that their appearance also is seasonally dependent. Natural mineral dust from the Sahara blows out over the Atlantic ocean and can be seen as the area with large τ_A on the west-coast of Africa. Industrial areas in eastern Asia produce high density of sulfate. Large τ_A in central Africa during February and August is a consequence of biomass burning. Sea salt is categorized as "Large aerosol" with a range in diameter from 0.2 to 2μm and causes the pattern over oceanic areas which gives an AOT between 0.1 - 0.2. A new model computation which include all the aerosol components, gives the result of S as shown in Figure 2.6. The pattern is similar to Figure 2.4

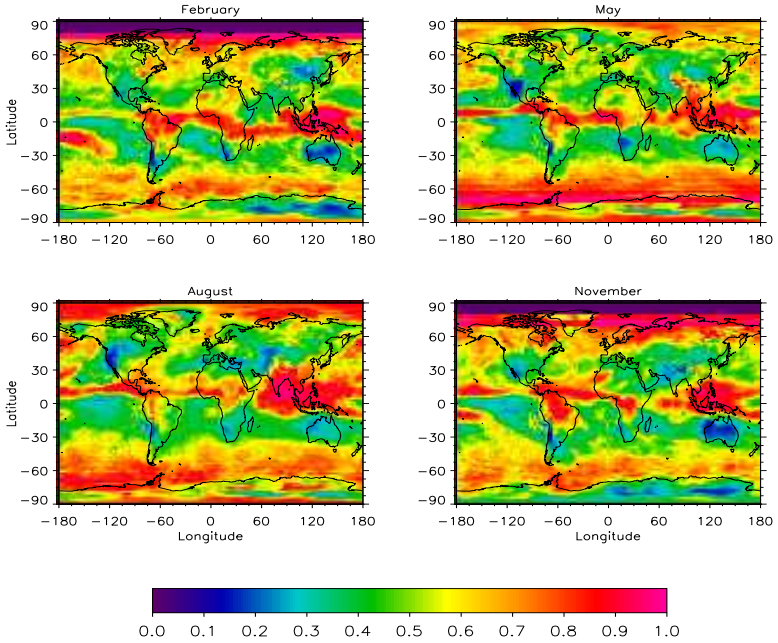

Figure 2.6: The seasonal variation of S with aerosols

in several areas since the cloud cover is the same, but the aerosols over the previous described areas have now changed the direct radiation into a diffuse component instead. S has increased over desert areas and reaches 0.4 - 0.5 in some regions. In the mid-latitude areas the difference is small, because of a small contribution from the aerosols. By including aerosols, the annual global mean flux at TOA increases by 2.4 W/m^2. The seasonal variation of S is strongest in Eastern parts of Asia and at mid-latitude. This is because of the seasonal dependence in clouds, as discussed above, and aerosols as well. The seasonal distribution of aerosols also changes the S over desert areas during the year, but since the effect of cloud cover here is small, the aerosols contribute to the change alone.

Chapter 3

Methods

3.1 MODIS

To investigate the surface albedo in this study, we use data from the MODerate resolution Imaging Spectroradiometer (MODIS) on NASA's TERRA satellite. MODIS has provided image spectroscopy since year 2000 and is used in several research projects concerning atmosphere, land and ocean. The satellite is sun-synchronous and the clear sky retrievals are taken near local solar noon. The horizontal spatial resolution of MODIS albedo data is 1 km and it takes the satellite 16 days to cover the whole earth. Accordingly, the retrievals are 16 - days means from each month. Among other products, MODIS provides both land cover and surface albedo data sets.

3.1.1 MODIS land cover product

The MODIS land cover product MOD12C1 is used to picture the Earth's vegetation canopy and include the International Geosphere - Biosphere Program (IGBP) scheme. This scheme divides all vegetation types into 18 classes as shown in Table 3.1. Figure 3.1 shows the global vegetation extension of each class. The main vegetation class in mid - latitude of NH is evergreen needle forest, and covers nearly 100 % of norhern parts of Europe. Other vegetation types that have a large global extend are open shrubland, grassland and cropland. Notice the extension of cropland which mainly concerns Europe, East Asia and North - America. Some vegetation types are known a priori like the well known deserts Sahara and Gobi, and they are seen in the barren or sparsely vegetated class. Tropical regions consist of large areas of shrubland and grassland. Central Africa has areas of dense evergreen broadleaf forest. The latter area is exposed to biomass burning and contribute to high density of aerosols, especially during August. The unclassified vegetation class is not included in the model since the extension of it is too low. The vegetation classes cropland, cropland mosaic and urban are referred to as anthropogenic vegetation, since the first appearance of these is not noticeable before the beginning of agricultural times.

The MODIS land cover product operates with a spatial resolution of $0.25° \times 0.25°$, and each pixel is described by a fraction of how much a grid box is covered by a special vegetation class. This means that any grid box can contain more than just one land cover class. The formula of computing surface albedo at each grid point is taken from Betts (2000), Equation 3.1.

$$\alpha = \alpha_0 + (\alpha_s - \alpha_0)(1 - e^{-0.2S_d}) \tag{3.1}$$

α_0 is the surface albedo for a given vegetation type of snow free condition, α_s is the surface albedo when snow appears. S_d is the snow depth. In this equation, α_s should be an upper limit on surface albedo during snow condition.

Vegetation number	Vegetation set
1	Evergreen Needleleaf
2	Evergreen Broadleaf
3	Deciduous Needleleaf
4	Deciduous Broadleaf
5	Mixed Forest
6	Closed Shrubland
7	Open Shrubland
8	Woody Savanna
9	Savanna
10	Grassland
11	Permanent Wetland
12	Cropland
13	Urban
14	Cropland Mosaic
15	Snow and Ice
16	Barren
17	Water
18	Unclassified

Table 3.1: The 18 IGBP land cover classes

3.1.2 MODIS surface albedo data

The MODIS surface albedo product MOD43C1(v004) (Schaaf, 2004) operates with two different surface albedos. Blacksky albedo is the surface albedo calculated without diffuse radiation (direct illumination). Whitesky albedo has a diffuse isotropic component and is also called bi - hemispherical reflectance. The actual surface albedo is a combination between the two albedo calculations. For both black- and whitesky albedo, the MODIS surface albedo product provides 7 spectral bands and three broadbands. The broadbands are 0.4 - 0.7μm (VIS), 0.7 - 5μm (IR), and 0.4 - 5μm (VIS and IR). In this study the focus is on the latter broadband.

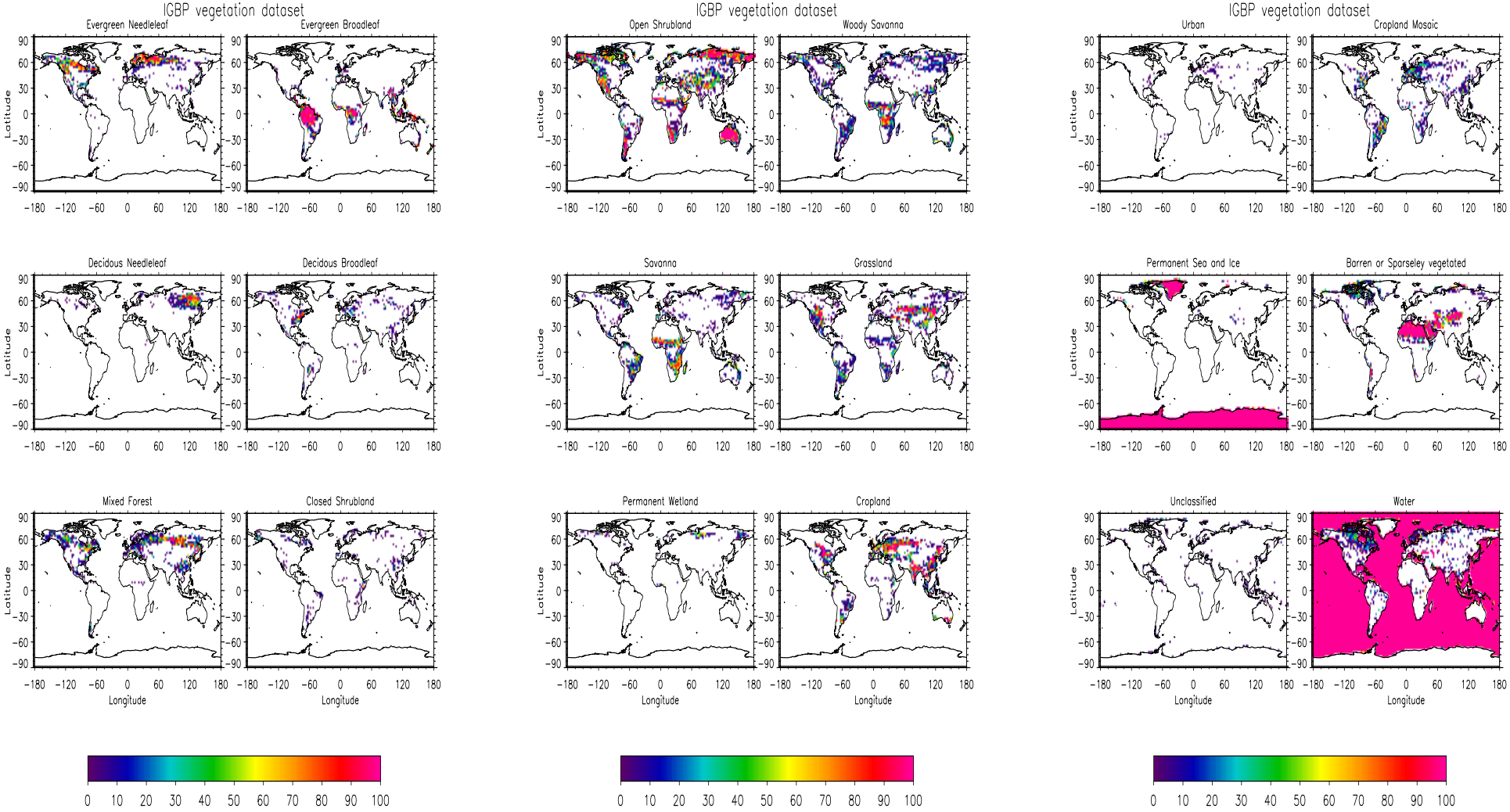

Figure 3.1: MODIS land cover classes 1-18

The MODIS surface albedo product has a spatial resolution of $0.05° \times 0.05°$. In order to make it fit the MODIS land cover product, the resolution is reduced to $0.25° \times 0.25°$. Figure 3.2 shows the satellite retrieval of blacksky and whitesky albedo from different months. The whitesky albedo data is generally higher (approximately 10 %) than the blacksky value. Some patterns are visible during the whole season such as the area with high surface albedo over North Africa, which is the Sahara. The albedo over South America remains constant during the season. The region in central Asia has almost an uniform albedo distribution during August except from a higher albedo in the Himalaya. Areas with major extend of forest are expected to have a relatively low albedo value compared to cropland and grassland. This is because of their high canopy density and shading properties. When we are looking at the difference between the blacksky and whitesky distribution, the most significant deviation is at higher latitude in NH winter because of the appearance of snow. Here the blacksky albedo is slightly higher than the whitesky albedo. The main pattern shows that the whitesky value is higher than the blacksky, especially in tropical regions in Africa and South - America.

3.2 Potential natural vegetation (PNV) data set

The changes in vegetation canopy from pre agricultural time are primarily due to forests that have been converted to cropland. By using historical data, Ramankutty and Foley (1999) represented the potential natrual vegetation data set with vegetation classes which vary somewhat from the IGBP scheme, i.e more accuracy in forests and without agriculture and urban classes. The global extension of the vegetation classes used in this data set is shown in Figure 3.3. Note the occurrence of forest vegetation in Europe and western parts of Asia. There are elements of grassland and shrubland vegetation in those areas as well. Northern parts of America also consist of different kinds of forests, except from an area of grassland/steppe in mid - America. The Amazon covers almost half of the northern parts of South - America. The PNV data set represents the natural pre agricultural vegetation that have most likely occurred there today with the same climate but without any anthropogenic disturbance. The anthropogenic IGBP vegetation classes cropland, cropland mosaic and urban are replaced in the model by vegetation set from the PNV.

3.3 Improvements

The improvements in this study include new vegetation and surface albedo data sets which is implemented in addition to earlier studies (Myhre and Myhre, 2003). MODIS vegetation and MODIS surface albedo data sets are used in the four improved surface albedo data sets.

3.3.1 Jin values

To improve the model with new surface albedo data, values from Jin et al. (2002) are implemented. The α_{jin} - values in Table 3.2 show the blacksky albedo means in a shortwave broadband (0.3 - 5.0μm) over 40° - 50°N

provided by Jin et al. (2002). This paper uses MODIS data from NH wintertime during November 2000 - January 2001. Both snow free and snow covered albedos are performed. Only the snow free albedo values are used in my improvement. For values not mentioned in Jin et al. (2002), the values from the study of Myhre and Myhre (2003) are used and performed for vegetation classes 2, 6, 11, 13, 15 and 17.

Vegetation set	α_{Jin}	α_{Zouh}
Evergreen Needleleaf (1)	0.105	0.110
Evergreen Broadleaf (2)	0.130	0.142
Deciduous Needleleaf (3)	0.127	0.126
Deciduous Broadleaf (4)	0.122	0.148
Mixed Forest(5)	0.112	0.132
Closed Shrubland (6)	0.218	0.151
Open Shrubland (7)	0.153	0.180
Woody Savanna (8)	0.137	0.136
Savanna (9)	0.142	0.152
Grassland (10)	0.169	0.176
Permanent Wetlands (11)	0.115	0.126
Cropland (12)	0.141	0.167
Urban (13)	0.170	0.146
Cropland Mosaic(14)	0.150	0.162
Snow and Ice (15)	0.832	0.617
Barren (16)	0.205	0.316
Water (17)	0.066	0.066

Table 3.2: Albedo values for snow free condition as represented by Jin et al. (2002) and Zouh et al. (2003)

Vegetation set	$snow_{max}$
Evergreen Needleleaf (1)	0.258
Evergreen Broaleaf (2)	0.260
Deciduous Needleleaf (3)	0.368
Deciduous Broadleaf (4)	0.310
Mixed Forest(5)	0.268
Close Shrubland(6)	0.600
Open Shrubland (7)	0.701
Woody Savanna (8)	0.386
Savanna (9)	0.600
Grassland (10)	0.729
Permanent Wetlands (11)	0.600
Cropland (12)	0.690
Urban (13)	0.480
Cropland Mosaic(14)	0.720
Snow and Ice (15)	0.780
Barren (16)	0.780
Water (17)	0.780

Table 3.3: Maximum albedo values for snow condition as represented by Gao et al. (2005) and Myhre and Myhre (2003)

As previously mention, the snow values should be a maximum value of each vegetation type, and for this purpose it must be a global mean. Gao et al. (2005) used Modis whitesky data in the retrieval of snow covered IGBP vegetation classes and found maximum values for different latitude broadbands. The maximum value from each latitude broadband is implemented as α_s in Equation 3.1. Gao et al. (2005) explored surface albedo values only for major vegetation types in the IGBP classes. For classes not mention in this paper, values from similar researches with data from the satellite instrument SARB are implemented, which also were used by Myhre and Myhre (2003). These classes are 2, 4, 6, 9, 11, 13, 15, 16 and 17. The maximum albedo values for all snow covered IGBP classes are listed in Table 3.3.

3.3.2 Zouh values

A comparison between MODIS albedo data and a common land model was publish by Zouh et al. (2003) and they represented the albedo as a blacksky retrieval in both visible (VIS) and near infrared (NIR) wavelengths. The weighted relationship between the two broadbands is in Equation 3.2. Zouh et al. (2003) analyzed the spatial albedo variation within the MODIS local noon blacksky albedo data set from 2001 (MOD43B3, v003).

$$\alpha_{zouh} = 0.465 \times \alpha_{vis} + 0.535 \times \alpha_{nir} \tag{3.2}$$

The values α_{vis} and α_{nir} which are applied to the model, are global averages starting at days of 193 - 214 and 17 - 65 in the NH an SH summer, respectively. The weights are based on incident solar radiation in their respective shortwave broadband. The computed α_{zouh} - values are shown in Table 3.2. This second attempt of calculating radiative forcing with new albedo values included the same snow cover values as in the first approach, see Table 3.3.

3.3.3 Comparison of Jin and Zouh

The α_{zouh} - values are generally higher than the α_{jin} - values. This is valid for all the vegetation types except from deciduous needleleaf and woody savanna, and for these two vegetation types, the difference is not significantly high (approximately 0.01). The higher albedo from Zouh et al. (2003) is caused by the difference of using mid - latitude winter albedo (Jin) in contrast to globally NH and SH summer albedo (Zouh). This specially influence the different values of cropland, 0.14 and 0.16, respectively, which Myhre and Myhre (2003) pointed out as a sensitivity factor in the calculation of radiative forcing.

3.3.4 This study

One way to improve the albedo values is to have a seasonal and regional variation in the albedo data. The power of this study is the usage of both vegetation and surface albedo from the same source, the MODIS satellite. Previous studies did not have this advantage and used different data sets (Hansen et al., 1998; Betts, 2001; Myhre and Myhre, 2003). MODIS surface albedo and MODIS land cover products have never been used coincidentally in a radiative forcing study.

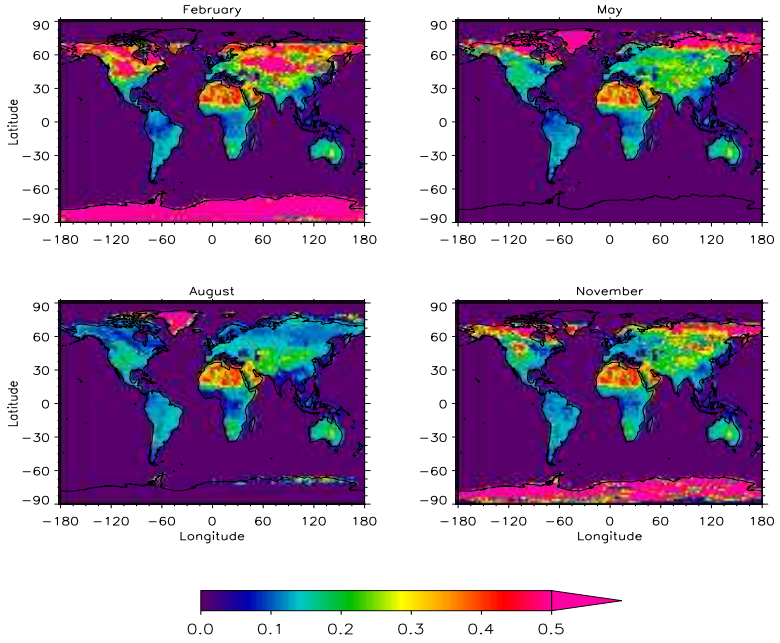

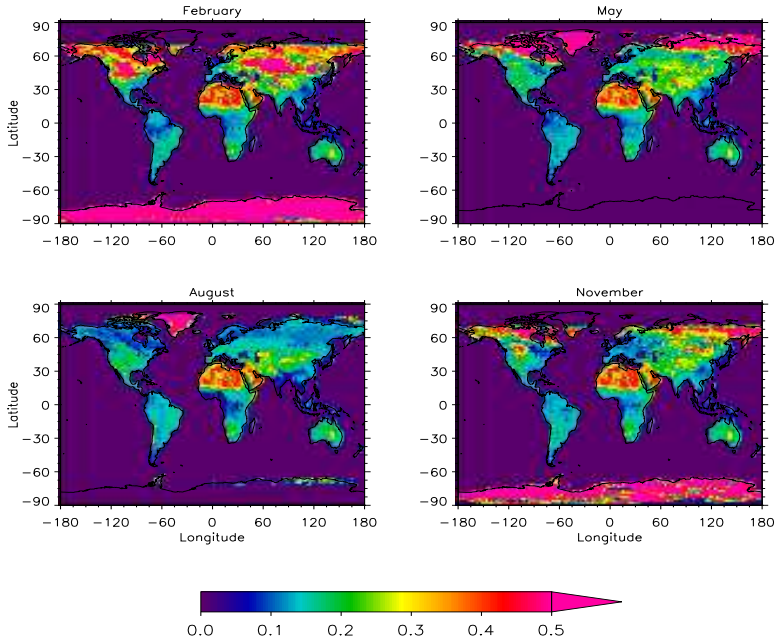

Figure 3.2: MODIS blacksky (above) and whitesky (below) with seasonal variation

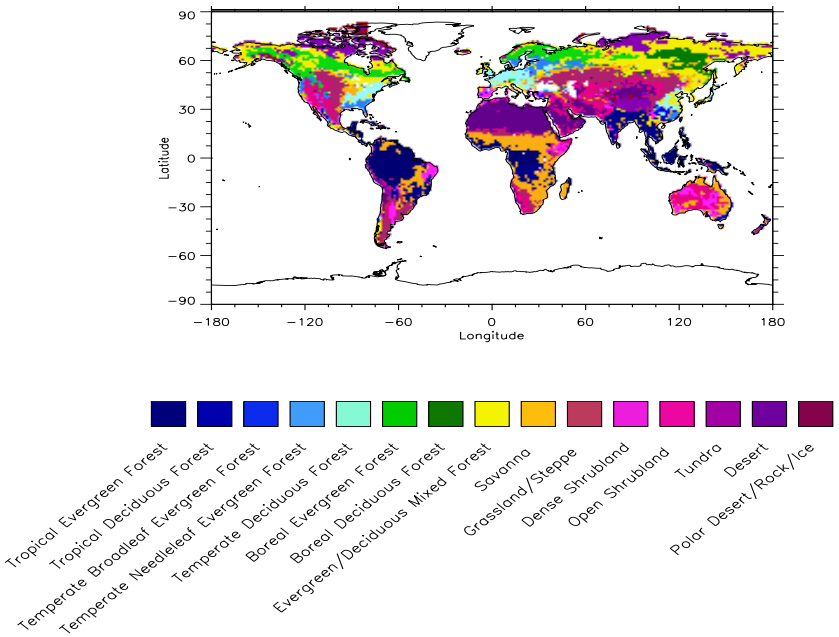

Figure 3.3: PNV classes given by Ramankutty and Foley (1999)

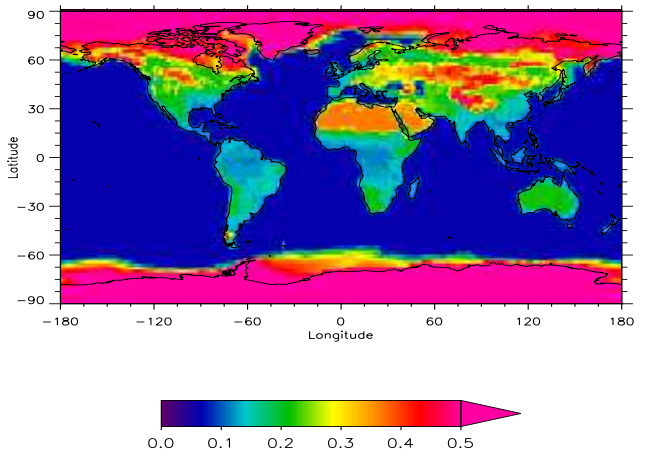

Figure 3.4: Annual surface albedo using MODIS land cover and surface albedo products for present time

Seasonal variation

Vegetation changes during the season. Deciduous leaves, crop diversity and snowfall are all factors that change the reflectance properties of the surface. For this reason, it is necessary to implement a seasonal variation of the MODIS surface albedo data. The year is split into four periods as follows: December/January/February (I), March/April/May (II), June/July/August (III), September/October/November (IV). Each season has an albedo which is represented by its last month and every month is a 16 - days mean. The retrieval of the 16 - day period in each month starts at Julian day 33, 129, 225 and 305 respectively. Data from the same period during four years, 2001 - 2004, is averaged and used as the albedo values for each season. May is represented by five years, 2000 - 2004. As mentioned earlier, the MODIS satellite has problems obtaining clear sky retrievals over India in August, and for that month, the albedo value is averaged over I, II and IV. This only concerns the cropland vegetation class.

Regional variation

Figure 3.1 shows the distribution of the 18 MODIS land cover classes. A single vegetation type may have different albedo in different parts of the world. Open Shrubland has an albedo close to 0.13 at lower latitudes and as high as 0.20 at higher latitudes. By dividing some of the vegetation classes into separate parts, it increases the accuracy of surface albedo in many areas. The separations are performed for evergreen broadleaf, open shrubland, cropland and barren. Evergreen broadleaf has different albedo in the Amazonas compared to the rest of the world, so this gives us a two separations. Open shrubland is divided into three separate parts: 35° - 45°N, Australia, and north and south of the longitude band. Cropland is divided into three regions which show dissimilarity in albedo even though they are set to be the same class by MODIS. The separation is done in Eurasia, East Asia/India, and the rest of the cropland areas which are not influenced by the two other regions. As seen in Figure 3.2, the Saharan and Arabian deserts have a high surface albedo. This is part of the barren vegetation class, and is separated into a single region. Barren in Asia is also separated because it contains the Gobi desert with a lower surface albedo than other barren parts in the world. The third barren region is areas which are not influenced by the two first separations.

Thresholds are made for the purpose of not influence the albedo values by snow. When averaging the albedo over larger areas, the MODIS surface albedo include snow covered areas as well. The vegetation classes with thresholds are the forests classes (1 - 5), open shrubland (7) at higher latitudes, grassland (10) and cropland (12). Their respective thresholds are 0.2, 0.25, 0.25 and [0.05, 0.25]. It is important to screen the data for snow in the Eurasian region for cropland in May . That is because there is a combination of snow free and snow covering areas. For that reason, the threshold is set to be 0.20.

The averaged surface albedo values are calculated in every grid box which is covered with more than 95 % of one single vegetation type. The vegetation class of cropland mosaic, no 14, has a relatively large global extend compared to some of the other classes, see Figure 3.1. Very few grid boxes contain more than 95 % of cropland mosaic, and because of this there is not enough points to make a verified value. Instead of using a value from previous studies, we apply cropland mosaic to cropland grid points. The method increases the reliability of the statistical material and uses approximately 45 % more grid points to average the MODIS values. The seasonal blacksky albedo values are shown in Table 3.4 and the whitesky values are listed in Table 3.5.

3.3.5 Blacksky and whitesky values

The forest classes in tables 3.4 - 3.5 operate with the lowest surface albedo values. Classes 1 - 3 have a blacksky and whitesky surface albedo of approximately 0.100 and 0.110, respectively, and deciduous broadleaf and mixed forest have albedo values approxmiately 0.01 higher. Open shrubland shows a significant variation between the three regions in which it is separated, and has the highest value during February in the latitudinal broadband. The surface albedo for cropland has a spatial variation within the three separated regions. Cropland areas which are not consider in the Eurasia or Asia class have the highest albedo among the three subclasses. The barren vegetation, class no 16, has a strong variation in surface albedo values between the three regions it is separated in. Areas not concerning Sahara, Arabia or Asia have the lowest surface albedo value with 0.174 - 0.182 (blacksky) and 0.179 - 0.183 (whitesky). According to the vegetation distribution, this concerns barren regions located at latitudes above 60°N. The albedo value for the Sahara and Arabia is the highest among all vegetation types, and is approximately 0.360.

The seasonal variation within the classes is most significant for vegetation types at mid - latitudes, i.e mixed forest, open shrubland, grassland and cropland. These vegetation types get influenced by snow during NH wintertime. Because of the thresholds due to screening the data for snow, the variation is caused by factors such as insolation, different types of crop in land use areas, rainfall and drought.

Classes not mentioned in tables 3.4 - 3.5 have their values from previous studies by Myhre and Myhre (2003). This is valid for classes no 6, 11, 13 and 15, and their seasonal independent snow free values are shown in Table 3.2.

Further improvements

Model outputs contain information of diffuse and direct radiation that reach the surface. This can be used in an interpolation between the two albedo data sets as shown in Equation 3.3 (Schaaf et al., 2002).

$$\alpha = S \times \alpha_{ws} + (1 - S) \times \alpha_{bs} \tag{3.3}$$

S is referred to as the relative diffuse radiation and is a monthly mean. The α_{ws}- and α_{bs} - values are the seasonal and regional averaged whitesky and

Vegetation set	February	May	August	November
Evergreen Needleleaf (1)	0.098	0.098	0.098	0.098
Evergreen Broadleaf in Amazon (2)	0.103	0.104	0.122	0.121
Evergreen Broadleaf exluding Amazon (2)	0.111	0.113	0.101	0.114
Deciduous Needleleaf (3)	0.108	0.108	0.108	0.108
Deciduous Broadleaf (4)	0.112	0.138	0.144	0.118
Mixed Forest(5)	0.120	0.126	0.119	0.115
Open Shrubland 35°S - 45°N (7)	0.223	0.218	0.208	0.218
Open Shrubland Australia (7)	0.175	0.174	0.177	0.173
Open Shrubland other	0.132	0.121	0.136	0.140
Woody Savanna (8)	0.118	0.118	0.103	0.122
Savanna (9)	0.138	0.143	0.119	0.133
Grassland (10)	0.188	0.186	0.166	0.184
Cropland Eurasia (12)	0.147	0.153	0.139	0.142
Cropland East Asia, India (12)	0.141	0.141	0.143	0.141
Cropland other (12)	0.153	0.149	0.153	0.155
Barren in Sahara and the Arabian desert (16)	0.368	0.357	0.354	0.367
Barren in Asia (16)	0.230	0.230	0.232	0.229
Barren excluding Sahara, the Arabian desert and Asia (16)	0.178	0.174	0.182	0.178

Table 3.4: The blacksky albedo values for the IGBP vegetation classes with seasonal variation

Vegetation set	February	May	August	November
Evergreen Needleleaf (1)	0.103	0.103	0.103	0.103
Evergreen Broadleaf in Amazon (2)	0.115	0.116	0.137	0.136
Evergreen Broadleaf excluding Amazon (2)	0.123	0.126	0.113	0.126
Deciduous Needleleaf (3)	0.112	0.112	0.112	0.112
Deciduous Broadleaf (4)	0.110	0.151	0.159	0.117
Mixed Forest(5)	0.123	0.132	0.128	0.110
Open Shrubland 35°S - 45°N (7)	0.234	0.233	0.225	0.229
Open Shrubland Australia (7)	0.190	0.182	0.185	0.185
Open Shrubland other (7)	0.134	0.119	0.136	0.148
Woody Savanna (8)	0.130	0.133	0.115	0.135
Savanna (9)	0.152	0.158	0.132	0.148
Grassland (10)	0.191	0.193	0.180	0.181
Cropland Eurasia (12)	0.152	0.162	0.154	0.139
Cropland East Asia, India (12)	0.150	0.148	0.150	0.151
Cropland other (12)	0.163	0.159	0.151	0.160
Barren in Sahara and the Arabian desert (16)	0.377	0.371	0.369	0.376
Barren in Asia (16)	0.241	0.245	0.249	0.229
Barren excluding the Arabian desert and Asia (16)	0.179	0.175	0.183	0.179

Table 3.5: The whitesky albedo values for the IGBP vegetation classes with seasonal variation

blacksky albedo, respectively. The next step to get a more realistic model is to include aerosols. Five kinds of aerosols are taken into account for the radiative transfer calculation, which is mentioned in chapter 2.5.2. Figure 3.4 shows the annual albedo distribution when using MODIS land cover and surface albedo data sets. We see how the global vegetation distribution determines the surface albedo. Sahara and Arabia have an albedo value of approximately 0.35. The Amazonas has a large extend of evergreen broadleaf with a surface albedo range from 0.11 to 0.13. High surface albedo in Eurasia and northern parts of America is caused by snow covered cropland and locally it reaches 0.5. Snow and ice cover over Arctic and Antarctica shows a surface albedo of approximately 0.6.

Self-composed albedo data set with MODIS data

The previous approaches included seasonal and regional averaged surface albedo values for each vegetation type. A better way of representing the present albedo is to directly use the satellite retrieved values for each pixel. Figure 1 in the appendix shows the global distribution of present surface albedo computed with MODIS data. We see the similarity between the calculated albedo and the whitesky and blacksky albedos in Figure 3.2. Equations 3.4 - 3.5 show how the new albedo for pre agricultural time is performed. We use the MODIS satellite data and subtract a calculated $\Delta albedo$ from it to perform a *pre albedo* data set representing the pre agricultural surface albedo. The data set given by Ramankutty and Foley (1999) is included in this method to obtain the $\Delta albedo$ in Equation 3.5. The anthropogenic influenced classes 12, 13 and 14 are replaced in *MODIS albedo* by classes from Ramankutty and Foley (1999).

$$pre\ albedo = MODIS\ albedo - \Delta albedo \tag{3.4}$$

$$\Delta albedo = MODIS\ albedo - PNV\ albedo \tag{3.5}$$

It is possible for the *pre albedo* to be negative in areas which previously have had a higher albedo than present, i.e forestation areas. That is because the $\Delta albedo$ is too high according to the MODIS data. To adjust for that, a lower limit is set for the albedo computed with the equations 3.4 - 3.5. The limit is found in the paper of Gao et al. (2005) which estimated the minimum global snow free whitesky albedo for the MODIS total shortwave broadband at all the IGBP vegetation classes. According to Gao et al. (2005) we put a constraint on the data set by not allowing the pre agricultural albedo to be lower than 0.081 in anthropogenic affected vegetation areas.

Chapter 4

Results

To quantify the radiative forcing due to changes in surface albedo caused by changes in vegetation, we can look at the balance between outgoing radiation at TOA from present and pre agricultural time represented by two surface albedo data sets. The conclusions will concern the four situations of (a) Jin, (b) Zouh, (c) the unconstrained MODIS approach and (d) the constrained MODIS approach. The letters refer to the sub-figures in Figure 4.1. The pattern in the results between the four different approaches is more or less the same, but the radiative forcing calculations due to the data sets deviate. All results are represented as annual global means, except in the discussion about seasonal variation.

4.1 Surface albedo changes

When analyzing the model results after the four main cases, we see the usual increase in surface albedo in areas in Europe, Eurasia, and northeast America. This is caused by deforestation and cultivation. The deviation is also perceptible in East Asia. Even though the results from the four data sets resemble each other, there are locally minor and major differences which become significant when calculating surface albedo difference and radiative forcing estimates.

4.1.1 Jin and Zouh

Figure 4.1 a) shows the annual distribution of the difference in surface albedo when using α_{jin} - values. Globally, the surface albedo has increased by 0.0013 during the period from pre agricultural time and until now. The annual maximum positive deviation within the data sets of Jin et al. (2002) is an albedo change of 0.16 in the agriculture Eurasian region, and the annual maximum reduction is approximately -0.06 in the northwest part of India and Pakistan. In the latter area, the pre agricultural data set operates with a vegetation of barren and open shrubland while MODIS consider this as cropland. This means a drop in surface albedo value of 0.064. The reason for a high annual mean surface albedo difference in Eurasia is due to the impact of snow covered ground. Compared to the figures of vegetation, Figure 3.1, we see that the highest increase of albedo is in areas which now are converted to cropland. For that reason, we may consider that the

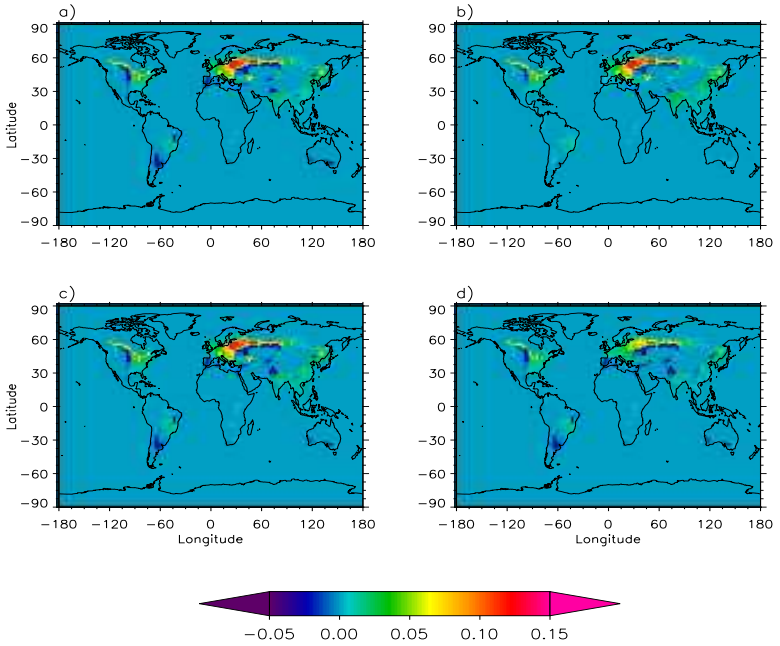

Figure 4.1: Annual mean albedo difference between present and pre agricultural time for four data sets

increase is caused by deforestation, since the PNV data set operates with a mixture of temperate needleleaf evergreen forest, temperate deciduous forest and evergreen/deciduous mixed forest in this region. A snow covered forest has a much lower albedo than snow covered cropland. According to Table 3.3, maximum albedo value of snow covered forests is approximately 0.30, but it reaches 0.69 for snow covered cropland. South of the pattern of highest increase in Eurasia, there is a following negative pattern. This is caused by the change of vegetation from grassland with surface albedo 0.169 to cropland with value 0.141 for α_{jin} - values, and from 0.176 to 0.167 for α_{zouh} - values. The negative pattern in South America is caused by grassland vegetation converted to cropland. For the Jin - approach it leads to a decrease of 0.028 in the surface albedo. In northern parts of America there is both an area of increasing albedo and a pattern with a negative difference in surface albedo. The positive albedo difference is caused by deforestation and is relatively high because of the influence of snow in NH wintertime. The negative pattern is due to grassland that has been converted to cropland and obtains the same negative surface albedo difference as in Eurasia.

Compared to the result using α_{zouh} - values in Figure 4.1 b), the albedo has increased by 0.0017 during the same period. Global positive and negative maximum albedo difference is 0.18 in the Eurasian region and -0.04 in the area described above in Pakistan, respectively. We see the same strong

positive albedo difference in Eurasian areas. The α_{zouh} - value of cropland is 0.167 which is higher than the value represented by Jin et al. (2002). There is a small difference on the east coast of South - America in the Zouh case compared to Jin, since the negative contribution to the difference in surface albedo here is missing. This can be explained by a low grassland value in the Jin approach (0.169) compared to Zouh (0.176) and by the fact that the difference between the grassland- and cropland-value in Zouh is less than in Jin. For the same reason, the negative pattern south of the strong increase in Eurasia is weaker. On the East coast of Asia the results are almost equal for the two approaches. The surface albedo difference here is approximately 0.02 - 0.03 in both cases. There is only a small increase in pixels that show a higher albedo difference with α_{zouh} - values than with the α_{jin} - values in this area. The North - American pattern is maintained in the two situations.

4.1.2 New surface albedo data set - unconstrained MODIS

Figure 4.1 c) shows the result from the calculation with the whitesky and blacksky surface albedo combined with the diffuse and direct radiation at BOA. The calculation of S also includes aerosols. Again we can recognize the same areas as in the previous situations and the pattern is equal to Figure 4.1 a). This is due to the similarity in cropland values which for this albedo data set ranges from 0.139 to 0.156 for the α_{bs} - values and from 0.153 to 0.171 for α_{ws} - values due to the seasonal variation. The annual global increase of albedo is 0.0013. In the specially high annual albedo difference area over Eastern Europe and the western part of Asia the albedo difference reaches the global positive maximum value 0.168. The minimum albedo difference is found in Pakistan as mentioned above, but the negative difference is stronger in this case and reaches -0.069. On the East coast of Asia there is an area with a positive albedo difference of approximately 0.02 - 0.03. This is also a region with high fraction of cropland vegetation, but the influence on the annual mean albedo difference is not so large since it is unaffected by snow in the NH winter-season because of a milder climate. The albedo difference distribution on the American continent is similar to the Jin - approach.

4.1.3 Constrained MODIS

Before constraining the *pre albedo* in the limited MODIS approach, the $\Delta albedo$ is calculated as a temporary surface albedo difference between present and pre agricultural time. The result will be equal to the unconstrained MODIS approach and the $\Delta albedo$ distribution will be equal to the surface albedo difference in Figure 4.1 c). After the constraint, the surface albedo difference will be as shown in Figure 4.1 d). The annual global increase of albedo during the period we are examining is 0.0007. This is much less than for the unconstrained MODIS approach and illustrates that the present surface albedo has been dramatically overestimated for that situation or that the pre agricultural data set has been underestimated. Because of the limitation on the pre agricultural albedo, by not allowing it go below 0.081, the surface albedo difference is globally reduced compared to the three other situations. Even over the previous maximum albedo difference area in Eurasia there has been a reduction by up to 50 %. The strong negative pattern below the

Eurasian positive belt, has not been subject to any major changes compared to the three previous results. In North - America there is a reduction in the positive albedo difference area. Other regions in the world are not that much affected by the constraint. A summary of the annual global surface albedo changes is listed in Table 4.1. Only the four approaches that have been discussed above are included.

Albedo data set	Surface albedo change
Jin	0.0013
Zouh	0.0017
MODIS Blacksky/whitesky (unconstrained)	0.0013
MODIS Blacksky/whitesky (constrained)	0.0007

Table 4.1: Results of annual global mean surface albedo change

4.2 Radiative forcing

The regions that contribute the strongest to the radiative forcing is similar to the case of surface albedo changes. According to Equation 2.8 the radiative forcing is negative if the reflected amount of sunlight is increasing during a certain time period. Consequently it leads to a global cooling since more reflected radiant energy reaches TOA instead of being used to heat the Earth and the lower atmosphere. The range of the forcing is from approximately -15 W/m^2 to 10 W/m^2, and only reaches extreme values in a few distinct regions.

The annual global radiative forcing from the Jin-approach is computed by the model to be -0.090 W/m^2 and the global distribution is shown in Figure 4.2 a). The strongest negative forcing comes from areas in the NH mid-latitude. This region contributes most to the calculated annual radiative forcing in all four situations. The result from computations with α_{zouh} - values shows a radiative forcing of -0.165 W/m^2 and is displayed in Figure 4.2 b). The radiative forcing from the unconstrained MODIS calculation in 4.2 c) is -0.089 W/m^2. The results in 4.2 d) is based on the constrained MODIS data set and shows a radiative forcing of -0.032 W/m^2.

Including aerosols in the model makes the radiative forcing calculations more complex because they interact with the atmosphere in several ways as discussed in Chapter 2.5.2. When it comes to radiative forcing they are weakening the forcing by about 10 % because of scattering and absorption in the atmosphere. Consequently they alter the fraction of diffuse radiation and change the distribution of whitesky and blacksky albedo. On the other hand, aerosols also reduce the incident solar radiation that reaches ground level and for that reason they make the surface albedo less efficient. As a whole, this will contribute to the global radiation balance as a weakening in the radiative forcing since the change in diffuse radiation has less effect compared to the others.

The calculated radiative forcing from different computations are summarized in Table 4.2. Here are also the results from the single blacksky or whitesky albedo computations with and without aerosols. Note that the combined whitesky/blacksky radiative forcing calculations are within the range of a single estimate. Table 4.2 also reveals how the aerosols weaken the results. The radiative forcing results which resemble each other the most are Jin, MODIS blacksky with aerosols, and the unconstrained MODIS blacksky/whitesky. This is because of the almost equal processing of the cropland-value. They all end up with a radiative forcing result of approximately -0.09 W/m^2. Combining cropland and cropland mosaic in the same class results in a weakening of the radiative forcing by 0.007 W/m^2. The reason for this is an increase of numbers of cropland pixels in the eastern parts of South-America. Since agricultural areas in Eurasia do not increase their amount of pixels equally, the influence of snow covered ground in this area becomes less significant.

Albedo data set	Radiative forcing (W/m^2)
Jin	−0.091
Zouh	−0.165
MODIS blacksky without aerosols	−0.097
MODIS whitesky without aerosols	−0.114
MODIS blacksky + whitesky without aerosols	−0.102
MODIS blacksky with aerosols	−0.087
MODIS whitesky with aerosols	−0.102
MODIS blacksky/whitesky with aerosols, unconstrained	−0.092
MODIS blacksky/whitesky with aerosols, unconstrained and combined veg no 12 and 14	−0.089
MODIS with constrained pre agricultural albedo and aerosols	−0.039
MODIS with constrained pre agricultural albedo, aerosols and combined veg 12 and 14	−0.032

Table 4.2: Results of annual global mean radiative forcing

4.2.1 Seasonal variation

The seasonal variation in the radiative forcing is shown in Figure 4.3 I - IV, and each sub-figure represents the four seasons described above. The difference is at it most during NH wintertime because of the snow covered surface. This has a great influence on the annual mean radiative forcing calculations.

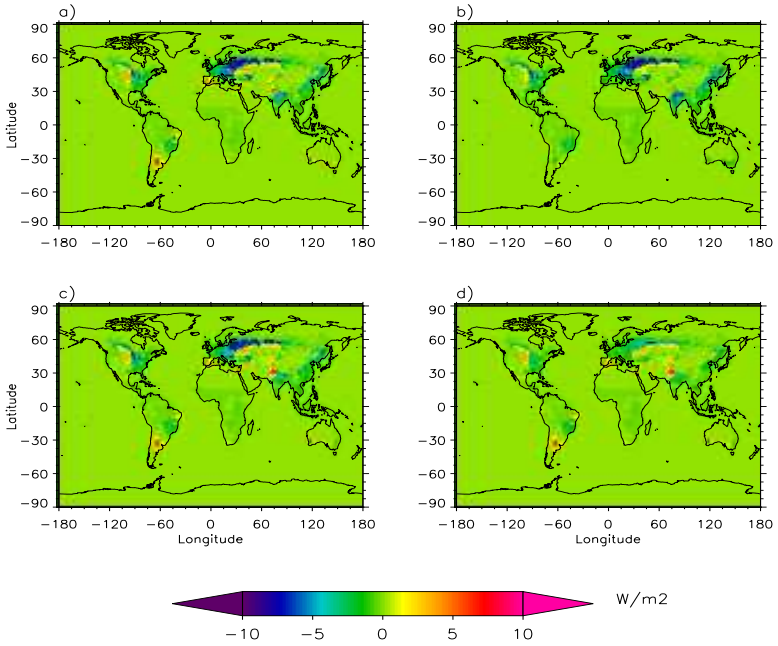

Figure 4.2: Annual mean radiative forcing between present and pre agricultural time for four data sets

In period I in Figure 4.3, the seasonal mean of short wave radiative forcing locally exceeds -15 W/m^2 in the mid-latitude European winter, agricultural regions in North - America and in Eastern Asia. This is a result of temperate needleleaf evergreen forest and temperate deciduous forest being replaced by cropland. Consequently, the snow albedos increase from 0.258 and 0.310, respectively, to cropland snow value 0.690 and hence the forcing to approximately -10 W/m^2. The positive pattern below the strong negative forcing in Eurasia is related to the decrease in albedo due to savanna and grassland vegetation which have been converted to cropland and is approximately 3 W/m^2. This area is also strongest during NH wintertime. From the seasonal variation, we clearly see how much the snow cover contributes to the radiative forcing estimation, but it is not required to get realistic results. An annual global mean will still catch the high influence of snow cover during NH winter because the agricultural areas in Eurasia always contribute most to the radiative forcing despite a seasonal variation.

4.2.2 Comparison with published results

My work has the advantage of using both MODIS vegetation and surface albedo products. A similar study has never been published before. Our best estimate of radiative forcing is much weaker than claimed earlier (Hansen et al., 1998; Betts, 2001; Myhre and Myhre, 2003; Matthews et al., 2003).

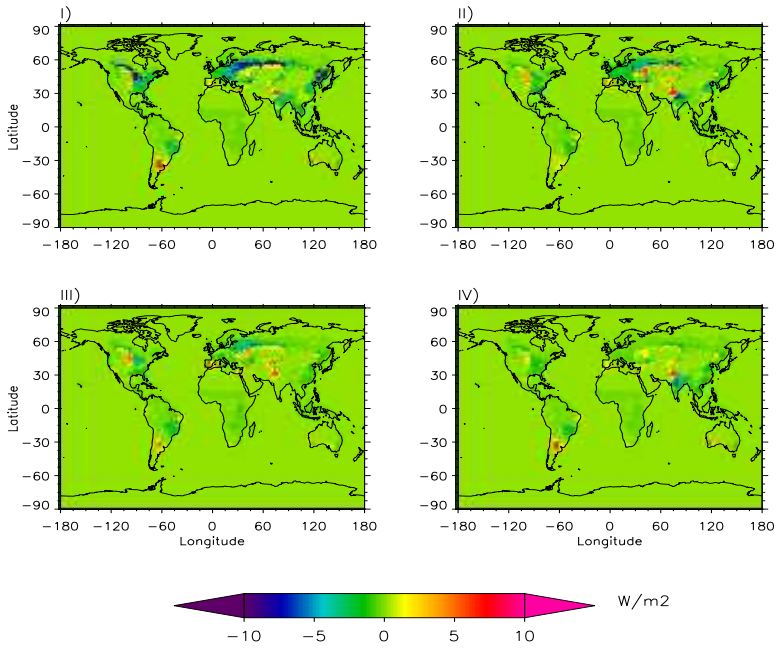

Figure 4.3: Seasonal variation in radiative forcing for the constrained MODIS data set

In this section, the goal is to illustrate how my result differs from published papers. The main difference is due to the choice of PNV data set and the surface albedo value of cropland.

A perspective done by Hansen et al. (1998), shows a radiative forcing between current and preindustrial time of -0.21 W/m^2. The pattern of the global distribution of the climate forcing shows highest contribution from Eurasia, North - America, West- and South Africa and in Eastern parts of Asia.

Betts (2001) used a potential natural state data set with no crop and an actual present-day vegetation from Wilson and Henderson-Sellers (1985) with a relatively high cropland albedo value (0.20). The main common features from the results in Betts (2001) are similiar to my approach. There is a strong radiative forcing in the Eurasian agricultural belt, North - America and East Asia. The forcing is stronger in Asia and North - America than in my study beacuse of the high value of cropland. The computed annual global radiative forcing due to these data sets is computed to be -0.20 W/m^2.

To see the effect of using different data sets for surface albedo and vegetation (both for current and PN vegetation), Myhre and Myhre (2003) combined some of the methods described above. The calculated radiative forcing

ranges from -0.66 to 0.28 W/m^2. A positive radiative forcing is caused by a data set with an unrealistically large change of surface albedo from arid regions in the Sahara and Arabian desert to cropland. The strongest negative radiative forcing estimate is from the vegetation data set by Goldewijk (2001) when pasture is excluded in barren regions combined with the surface albedo data set from Wilson and Henderson-Sellers (1985). In the study by Myhre and Myhre (2003), a global surface albedo increase of 0.01 is performed. For a cloud-free calculation the albedo increase is only carried out for the snow-free surface albedo values. It causes a stronger radiative forcing in tropical regions and a weakening to wards northern latitudes. When clouds are present in the model, the surface albedo increase causes another forcing pattern. Still there is no increase of snow albedo values in the model, but the forcing becomes globally weaker than in the first simulation. That is because incoming solar radiation that reach the surface is less than in the clear-sky calculation. Highest impact of clouds is seen in mid-latitudes and around Equator. Both areas show a weakening in the radiative forcing. Arid regions, Sahara and Arabian desert, show only smaller difference due to cloud-free calculation because of low cloud cover. The last approach in this sensitivity study by Myhre and Myhre (2003) includes an increase of surface albedo of 0.01 for both snow- and snow free values. Now the radiative forcing is strengthened in NH mid-latitude as well, but areas around Equator stay unchanged compared to the previous approach. This sensitivity study shows that albedo values for snow covered vegetation and realistic cloud cover are important factors for the global radiative forcing estimation. Related to my study of surface albedo changes caused by vegetation changes, the study by Myhre and Myhre (2003) shows that much more must be done to reduce the uncertainty because of snow cover since it is the NH mid-latitude that contributes most to the radiative forcing.

A paper by Matthews et al. (2003) used a vegetation data set based on a vegetation field from DeFries and Townsend (1994). The data set included only seven vegetation classes, and the cropland surface albedo from Sellers (1996) was set to be 0.17. To calculate radiative forcing estimates, the data set represented by Ramankutty and Foley (1999) for potential or natural vegetation field from year 1700 is used. The forcing estimate resulting from land cover change is reported to be -0.15 W/m^2. To investigate how the forcing is effected by an increase of surface albedo, he let the value of cropland be 0.20 for a transient run. This change resulted in a forcing of - 0.28 W/m^2.

Note that Hansen et al. (1998) calculated radiative forcing due to changes in surface albedo from pre industrial time, while results from Matthews et al. (2003), Myhre and Myhre (2003) and my study perform forcing calculations between present and pre agricultural time. Myhre and Myhre (2003) indicated that about 1/3 of the contribution to the present focing has its origin before 1750.

Chapter 5

Summary

Various types of MODIS data sets are used to investigate the effects on climate caused by surface albedo and vegetation changes. Two data sets from previous studies (Jin et al., 2002; Zouh et al., 2003) are adopted. Additionally, a third data set is made from MODIS land cover and MODIS surface albedo products and is later improved to perform a fourth data set. They are all used in a radiative forcing calculation in order to find the effect of replacing forest areas with agricultural crops. A potential natural vegetation data set from Ramankutty and Foley (1999) describes the vegetation canopy without any human disturbance. The effect of deforestation is explained through the net flux at TOA between pre agricultural and present times.

The surface albedo data set from Jin et al. (2002) includes MODIS blacksky albedo from a short wave broad band mean over 40° - 50°N in the NH winter period. The averaged surface albedos are assigned to 11 of the 18 different vegetation types from the IGBP scheme. From the calculation with the Jin et al. (2002) values, the radiative forcing results in a global cooling of -0.091 W/m^2. Zouh et al. (2003) operates with a NH and SH summertime surface albedo to average the albedo values for 16 vegetation types and has the highest snow free value for cropland (0.167). As a consequence, this results in the strongest radiative forcing estimate of -0.165 W/m^2. The third approach uses the surface albedo and land cover products from MODIS to compute a modified surface albedo. Data sets from MODIS surface albedo 16 - day retrievals during February, May, August and November in 2001-2004 have been used. MODIS provides both blacksky and whitesky surface albedo data sets in order to represent the direct and diffuse components of radiation, respectively. Both blacksky and whitesky albedo, with seasonal variation, are assigned to each of the 18 vegetation classes. Some of the vegetation classes have regional variation within the same class. For that reason, sub-classes for four of the vegetation types are performed. In the radiative transfer calculation, the actual albedo is computed by a combination of blacksky and whitesky albedos. In addition to calculating net flux at TOA, model outputs also contain information on the amount of diffuse and direct radiation that reaches the Earth's surface. The ratio between diffuse and total radiation at ground level is used in a calculation of a relative variable, S, which range from 0 to 1. Scattering and absorption from clouds, aerosols, and gases in the atmosphere affect the global distribution

of S. For that reason, five types of aerosols are included in the model: mineral dust, sea salt, black carbon, organic carbonaceous, and sulfate. The aerosols contribute to a high S - value especially over the Sahara and the industrial areas in Europe and Eastern Asia. The resultant radiative forcing value using the unconstrained MODIS data set is -0.09 W/m^2. To improve the self-composed surface albedo data set, a constraint is done for the purpose of avoiding an underestimation of the pre agricultural albedo. MODIS blacksky and whitesky albedo in combination with S describes the present surface albedo. In this case, no land cover data set is used, only observational MODIS surface albedo data. The limit is set to be 0.081 on the pre agricultural surface albedo. Because of this constraint, the radiative forcing is weaker than for the unconstrained situation and is now computed to be -0.03 W/m^2.

The estimations of radiative forcing show a variation from -0.032 to -0.165 W/m^2 according to the different data sets, which means that the Earth is less influenced by surface albedo changes than what has been earlier claimed. The most reliable and realistic estimate is from the computation with the self-composed pre agricultural albedo. Here the results show a radiative forcing of -0.032 W/m^2. The data set from MODIS in this study operates with a relatively low cropland albedo value compared to others (Jin et al., 2002; Zouh et al., 2003; Gao et al., 2005), see tables 3.4 - 3.5. In the unconstrained combined whitesky/blacksky estimation, it is presumed that either present albedo is overestimated or pre agricultural albedo is underestimated. Both effects are improved in the fourth approach by exluding the land cover data in the representation of the present albedo and by the constraint on the pre agricultural data set. Areas which contribute most to the radiative forcing calculation are agricultural regions in Eurasia and North America. This is caused by two effects which increase the surface albedo: Firstly, these areas have been deforested and trees have been replaced by cropland. Secondly, the regions are covered with snow during NH wintertime. Compared to other studies (Hansen et al., 1998; Betts, 2001), my results show similar patterns. The best estimate of the radiative forcing in this study is within the IPCC (2001) range, though weaker.

The conclusions of my study do not only consider a reduction in the uncertainty of radiative forcing due to vegetation changes, but there has also been an improvement in the estimation of the value of cropland. The two results are related, since an incorrect value of cropland may lead to a wrong radiative forcing, but we now claim the best estimate of cropland value to be 0.15.

The data set for pre agricultural surface albedo also shows improvement compared to previous studies. The constraint allows us to set a lower limit on the surface albedo and avoids an unrealistic high difference between forest regions in pre agricultural time and present-times crops. The result of the constraint is a 50 % reduction of the radiative forcing compared to our former results, especially in the eastern parts of Europe.

The MODIS surface albedo and land cover products appear to be a good combination in estimating radiative forcing. Further improvement can also be made by using the MODIS snow cover product (Hall and Riggs, 2002).

Bibliography

Aoki, T.; Hachikubo, A. and M.Hori (2003) *Effects of snow physical parameters on shortwave broadband albedos*. J. Geophys. Res., volume 108, NO. D19, 4616, doi:10.1029/2003JD003506.

Betts, R. (2000) *Offset of the potential carbon sink from boreal forestation by decreases in surface albedo*. Nature, volume 408:pp. 187–190.

Betts, R. (2001) *Biogeophysical impacts of land use on present day climate: near-surface temperature change and radiative forcing*. Atmos. Sci. Lett., volume 2:pp. 29–42.

DeFries, R. and Townsend, J. (1994) *NDVI - derived land cover classification at global scales*. Int. J. Remote Sensing, volume 15:pp. 3567 – 3586.

Gao, F.; Schaaf, C. and Strahler, A. (2005) *MODIS bidirectional reflectance distributionfunction and albedo Climate MOdeling Grid product and the variability of albedo for major global vegetation types*. J. Geophys. Res., volume 110, NO. D01104, doi:10.1029/2004JD005190.

Goldewijk, K. K. (2001) *Estimating global land use change over the past 300 years: The HYDE database*. Global Biogeochem. Cycles, volume 15:pp. 417–434.

Hall, D. and Riggs, G. (2002) *MODIS snow-cover products*. Remote Sens. Environ., volume 83:pp. 181–194.

Hansen, J.; Sato, M.; Lacis, A.; Ruedy, R.; Tegen, I. and E.Matthews (1998) *Climate forcings in the Industrial era*. Proc. Natl. Acad. Sci. USA, volume 95:pp. 12 753–12 758.

Henderson-Sellers, A. (1995) *Human effects on climate through the large-scale impacts of land-use change*, volume 16 (Future climate of the World).

IPCC (2001) *Radiative forcing of Climate Change*. Intergovernmental Panel on Climate Change IPCC.

Jin, Y.; Schaaf, C. and Gao, F. (2003) *Consistency of MODIS surface bidirectional reflectance distribution function and albedo retrievals: 1*. J. Geophys. Res., volume 108, NO. D5, 4158, doi:10.1029/2002JD002803.

Jin, Y.; Schaaf, C. B.; Gao, F.; Li, X. and Strahler, A. H. (2002) *How does snow impact the albedo of vegetated land surfaces as analyzed with MODIS data?*. Geophys. Res. Lett., volume 29, NO. 10, 10.1029/2001GL014132.

Liou, K. N. (2002) *An Introduction to Atmospheric Radiation*. International Geophysics Series (Academic Press), 2nd edition.

Matthews, D.; Weqver, A.; Eby, M. and Meissner, K. J. (2003) *Radiative forcing of climate by historical land cover change*. Geophys. Res. Lett., volume 30, NO. 2, 1055, doi:10.1029/2002GL016098.

Matthews, E. (1983) *Global vegetation and land use: New High - resolution data bases for climate studies*. J. Climate Appl. Meteor., volume 22:pp. 474–487.

Myhre, G. and Myhre, A. (2003) *Uncertainties in Radiative Forcing due to Surface Albedo Changes Caused by Land-Use Changes*. J. Climate, volume 16:pp. 1511–1524.

Myhre, G. and Stordal, F. (2001) *On the tradeoff of the solar and thermal infrared radiative impact of contrails*. Geophys. Res. Lett., volume 28(16):pp. 3119–3122.

Ramankutty, N. and Foley, J.A (1999) *Estimating historical changes in global land cover:Croplands from 1700 to 1992*. Global Biogeochem. Cycles, volume 13(4):pp. 997–1027.

Schaaf, C. (2004) *MOD43 BRDF/Albedo Product*. Webpage. URL `http://geography.bu.edu/brdf/product.html`.

Schaaf, C.; Gao, F.; Strahler, A. H. and Lucht, W. (2002) *First operational BRDF, albedo nadir reflectance products from MODIS*. Remote Sens. Environ., volume 83:pp. 135–148.

Sellers, P. (1996) *The ISLSCP initiativeI global dataset: Surface boundary conditions and atmospheric forcings for land-atmosphere studies*. Am. Met. Soc., volume 77:pp. 1987 – 2005.

Stamnes, K.; Tsay, S.C.; Wiscombe, W. and Jayaweera, K. (1988) *A numarically stable algorithm for discrete-ordinaet-method radiative transfer in multiple scattering and emmitting layered media*. Applied optics, volume 27:pp. 2502–2509.

Thomas, G. E. and Stamnes, K. (1999) *Radiative Transfer in the Atmosphere and Ocean*. Cambridge Atmospheric and Space Science Series (Cambridge University Press).

Wilson, M. F. and Henderson-Sellers, A. F. (1985) *A global archive of land cover and soils data for use in general circulation climate models*. J. Climatol, volume 5:pp. 119 – 143.

Zouh, L.; Dickinson, R.E.; Tian, Y. and Zeng, X. (2003) *Comparison of seasonal and spatial variations of albedos from Moderate-Resolution Imaging Spectrometer (MODIS) and Common Land Model*. J. Geophys. Res., volume 108, NO. D15,4488, doi:10.1029/2002JD003326.

Radiative forcing due to surface albedo change based on MODIS data

Gunnar Myhre[1,2], Maria M. Kvalevåg[1], Crystal B. Schaaf[3]

[1]Department of Geosciences, University of Oslo, 0315 Oslo, Norway
[2]Center for International Climate and Environmental Research – Oslo, 0318 Oslo, Norway
[3]Department of Geography, Boston University, MA 02215 USA

Abstract

In this study we use the capabilities of the MODIS land surface product to estimate the radiative forcing due to surface albedo changes caused by vegetation changes. We improve the representation of the present surface albedo by using data retrieved from MODIS. The change in surface albedo is based on the vegetation land cover from MODIS, a data set for potential natural vegetation, and surface albedo for the vegetation types derived from the MODIS data. We arrive at a radiative forcing due to surface albedo changes of -0.03 Wm^{-2}, weaker than most earlier published results for this climate forcing mechanism. This is mainly due to a lower surface albedo of cropland and further that the MODIS data allow us to constrain the surface albedo change.

1. Introduction

Radiative forcing of surface albedo changes caused by land use changes is quite uncertain but given a best estimate since pre-industrial time of -0.2 Wm^{-2} in IPCC (2001), with a range from 0 to -0.4 Wm^{-2}. The land use changes that are taken into account are mainly for agricultural activity with deforestation as the major cause. An essential role for the magnitude of the forcing is the much higher albedo for snow-covered non-forested regions than for forested areas [*Betts*, 2000, 2001; *Hansen, et al.*, 1998]. [*Myhre and Myhre*, 2003] found in a sensitivity study a somewhat larger range of likely radiative forcing from this mechanism than in IPCC (2001), and a positive forcing was not ruled out although not very probable. Several vegetation data sets and surface albedo sets for vegetation types was investigated in the sensitivity study. Importantly, the main cause for the relatively large range in the radiative forcing was owing to the surface albedo of cropland. The significance of the cropland surface albedo was illustrated by using 3 values (0.15, 0.18, and 0.20) based on published results [*Myhre and Myhre*, 2003]. In the experiment where only the cropland surface albedo was changed the resulting radiative forcing was -0.06, -0.20, and -0.29 Wm^{-2}, respectively. Similar result was found in [*Matthews, et al.*, 2003] where simulations were performed for cropland surface albedo of 0.17 to 0.20 with corresponding radiative forcing of -0.15 and -0.28 Wm^{-2}, respectively.

Earlier studies of radiative forcing due to albedo changes are based on vegetation data and associated surface albedo data for each of the vegetation types. These surface albedo data for each vegetation types have been treated as constant values. Some recent studies have analyzed the MODIS data and found surface albedo values for various vegetation types [*Gao, et al.*, 2005; *Jin, et al.*, 2002; *Zhou, et al.*, 2003]. In two of these studies[*Gao, et al.*, 2005; *Jin, et al.*, 2002] investigations of the impact of snow cover on the surface albedo have been made. This important effect for the surface albedo change is complicated as it not only differ for various vegetation types but also on a wide range of factors such as snow depth, time since last snow fall, and history of temperature and wind since last snow fall [*Aoki, et al.*, 2003].

Here we use the MODIS satellite product for the current surface albedo [*Schaaf, et al.*, 2002] and combine that with the MODIS vegetation data along with surface albedo with regional variation for the estimation of the pre-agriculture albedo. With this approach the current surface albedo is much better characterized than in earlier studies and this allow us to constrain the change in surface albedo from the vegetation changes.

2. The MODIS surface albedo and vegetation product

For the present surface albedo the MODIS product of white sky (completely diffuse) and black sky (direct beam) is adopted. In this study we have used 4 years of data (2001-2004) for a 16 days mean for 4 months. The four chosen months are used to represent the four seasons. The white sky and black sky albedo values are combined to an actual surface albedo and here information from the radiative transfer model has been used (see below). The present surface albedo from the MODIS is shown in Figure 1. Over ocean and in the polar night predefined values have been set. The figure shows clearly the high surface albedo over desert areas, but also differences in the surface albedo in arid regions. A minimum in the surface albedo is in tropical regions. At northern mid latitudes relatively high surface albedo is found due to snow cover during the winter season.

To establish change in the surface albedo from vegetation changes three IGBP classes of anthropogenic activity has been considered (cropland, urban, and cropland mosaic). Only in regions with MODIS vegetation data of these three classes surface albedo change have been performed. The MODIS vegetation has fractional data on a 0.25 degree resolution for 18 vegetation classes (see Table 1). In areas with anthropogenic influence on the vegetation cover (the three above mentioned classes) the vegetation cover has been replaced by the potential natural vegetation cover given by [*Ramankutty and Foley*, 1998]. To calculate the difference in the surface albedo (based on current MODIS vegetation data of anthropogenic vegetation and potential natural vegetation) we use the advantage of MODIS having surface albedo and vegetation cover products. Seasonal and regional (if necessary) information has been established in regions having more than 95% of a single vegetation type. To avoid snow influence on the analysis we have put threshold values on the surface albedo. The result of the investigation for the black sky albedo is shown in Table 1. Similar analysis for the white sky albedo shows generally 10% higher values compared to the black sky albedo. Importantly the surface albedo for cropland is relatively low (0.14-0.16) in accordance with other studies analyzing the

MODIS data [*Gao, et al.*, 2005; *Jin, et al.*, 2002; *Zhou, et al.*, 2003]. Some regional and seasonal variations in the surface albedo for the anthropogenic influenced vegetation types can be seen although not major differences (less than 10%). However, for some of the other vegetation types important regional differences have been implemented. The seasonal (and sometimes regional) varying black sky surface albedo (Table 1) and white sky surface albedo are essential for the calculation of change in the surface albedo.

An important constrain on the change in surface albedo is that we allow the pre-agriculture not to be lower than 0.081 in anthropogenic affected vegetation areas. This lower bound is based on minimum surface albedo values found in [*Gao, et al.*, 2005]. The importance of this lower bound is due to the use of the current surface albedo retrieved from MODIS in this study and thereafter subtract the human influenced (mainly deforestation) change in surface albedo. Without this constraint in the pre-agriculture surface albedo unrealistic low values may occur.

3. Radiative transfer model

An atmospheric radiative transfer code using the discrete ordinate method [*Myhre and Myhre*, 2003; *Stamnes, et al.*, 1988] is adopted for the radiative forcing calculations. The model includes absorption by atmospheric gases, Rayleigh scattering, scattering by clouds, and absorption and scattering by aerosols. Simulations have been performed with eight streams.

The meteorological data used in the radiative transfer calculations are from the European Centre for Medium-range Weather Forecasts (ECMWF). Monthly mean data for water vapour, clouds, snow depth, and snow cover are used. Treatment of the surface albedo when snow is present has been made as in [*Myhre and Myhre*, 2003]. Data for 5 aerosol types (sea salt, mineral dust, sulfate, black carbon, and organic carbon) as monthly mean are based on simulation from a chemistry transport model involved in a global aerosol intercomparison study (http://nansen.ipsl.jussieu.fr/AEROCOM). The meteorological data represent the year 1996 and simulations are performed on a T63 resolution (about 1.9x1.9 degrees).

The surface albedo, α, is calculated from an interpolation of the black sky and white sky albedo with the formula [*Schaaf, et al.*, 2002]

$$\alpha = (1\text{-}S)\,\alpha_{bs} + S\,\alpha_{ws} \qquad (1)$$

where α_{bs} is the black sky albedo, α_{ws} is the white sky albedo, and S is the fraction of diffuse sunlight reaching the surface. All these variables have important geographical variations. The geographical distributions of diffuse and direct sunlight have been calculated with the radiative transfer code for each month. In the calculation of S it is important with scattering and absorbing media in the atmosphere to be well represented.

4. Results

Figure 2 shows the calculated change in surface albedo caused by the vegetation changes. The usual increase in the surface albedo at mid-latitudes in the northern hemisphere can easily been seen. This is a result of deforestation for agricultural activity. The increase of the annual mean surface albedo is more than 0.1 in certain areas and is larger over Europe than in the North-America. In some areas the conversion of grassland to cropland has reduced the surface albedo, but of smaller magnitude than in region with deforestation. In northwestern part of India and Pakistan a decrease of the surface albedo is simulated, but this is due to the potential natural vegetation data indicate shrubland and even some small barren areas in this region. In all cases with a decrease of the surface albedo the simulated pre-agricultural surface albedo is not unrealistic high. The impact of constraining the surface albedo change (not allow the pre-agricultural surface albedo to be below 0.081) is to reduce the change significantly over Europe. This is especially over the eastern part of Europe where the change is reduced by around 50%. In other regions the impact of constraining the surface albedo is of much less importance.

The radiative forcing for the simulated change in surface albedo is shown in Figure 3. The pattern in the radiative forcing is similar to the pattern of the change in the albedo, but modification in the surface albedo results in a larger radiative forcing in tropical areas compared to at mid and high latitudes [*Myhre and Myhre*, 2003]. Radiative forcing is with a few exceptions within a magnitude of 10 Wm^{-2}. Compared to earlier studies the pattern of the radiative forcing is rather similar [*Betts*, 2001; *Hansen, et al.*, 1998; *Myhre and Myhre*, 2003]. The global and annual mean radiative forcing is calculated to be -0.03 Wm^{-2}, within the range given in IPCC (2001) but significantly weaker than the best estimate. Without constraining the surface albedo change we arrive at a radiative forcing of -0.09 Wm^{-2}.

Aerosols (of natural and anthropogenic sources) reduce the incoming solar radiation by scattering and absorption. This weakens the radiative forcing due to surface albedo by about 10%. However, it also alters the fraction of diffuse radiation that is of importance for the distribution of white sky and black sky albedo. This effect strengthens the radiative forcing due to surface albedo change but is a small effect compared to the shielding effect of solar radiation by the aerosols.

5. Summary

The main finding from this study is that radiative forcing from surface albedo changes caused by vegetation changes is generally weaker than found in earlier studies. This is mainly due to lower surface albedo for cropland, but also that we in addition constrain the surface albedo change by using the present surface albedo from MODIS and the limit on the pre-agricultural surface albedo. The first of these results in a radiative forcing of -0.09 Wm^{-2} whereas in the latter as we see as our best estimate results in a radiative forcing of -0.03 Wm^{-2}. The importance of constraining the surface albedo change is due to limited knowledge about the influence of snow cover.

Note that our radiative forcing estimate is since pre-agricultural time whereas since pre-industrial time as given in IPCC (2001). Typically one third of the radiative forcing due to surface albedo changes caused by vegetation changes have occurred before the beginning of the industrialization [*Myhre and Myhre*, 2003].

References

Aoki, T., et al. (2003), Effects of snow physical parameters on shortwave broadband albedos, *Journal Of Geophysical Research-Atmospheres*, *108*.

Betts, R. A. (2000), Offset of the potential carbon sink from boreal forestation by decreases in surface albedo, *Nature*, *408*, 187-190.

Betts, R. A. (2001), Biogeophysical impacts of land use on present-day climate: Near surface temperature change and radiative forcing, *Atmos. Sci. Lett.*, *2*, doi:10.1006/asle.2000.0023.

Gao, F., et al. (2005), MODIS bidirectional reflectance distribution function and albedo Climate Modeling Grid products and the variability of albedo for major global vegetation types, *Journal Of Geophysical Research-Atmospheres*, *110*.

Hansen, J. E., et al. (1998), Climate forcings in the Industrial era, *Proceedings Of The National Academy Of Sciences Of The United States Of America*, *95*, 12753-12758.

Jin, Y. F., et al. (2002), How does snow impact the albedo of vegetated land surfaces as analyzed with MODIS data? *Geophysical Research Letters*, *29*.

Matthews, H. D., et al. (2003), Radiative forcing of climate by historical land cover change, *Geophysical Research Letters*, *30*.

Myhre, G., and A. Myhre (2003), Uncertainties in radiative forcing due to surface albedo changes caused by land-use changes, *Journal Of Climate*, *16*, 1511-1524.

Ramankutty, N., and J. A. Foley (1998), Characterizing patterns of global land use: An analysis of global croplands data, *Global Biogeochemical Cycles*, *12*, 667-685.

Schaaf, C. B., et al. (2002), First operational BRDF, albedo nadir reflectance products from MODIS, *Remote Sensing Of Environment*, *83*, 135-148.

Stamnes, K., et al. (1988), Numerically Stable Algorithm For Discrete-Ordinate-Method Radiative-Transfer In Multiple-Scattering And Emitting Layered Media, *Applied Optics*, *27*, 2502-2509.

Zhou, L., et al. (2003), Comparison of seasonal and spatial variations of albedos from Moderate-Resolution Imaging Spectroradiometer (MODIS) and Common Land Model, *Journal Of Geophysical Research-Atmospheres*, *108*.

Vegetation set	February	May	August	November
Evergreen Needleleaf (1)	0.098	0.098	0.098	0.098
Evergreen Broadleaf in Amazonas (2)	0.103	0.104	0.122	0.121
Evergreen Broadleaf excluding Amazonas (2)	0.111	0.113	0.101	0.114
Decidious Needleleaf (3)	0.108	0.108	0.108	0.108
Decidious Broadleaf (4)	0.112	0.138	0.144	0.118
Mixed Forest(5)	0.120	0.126	0.119	0.115
Open Shrubland 35S-45N (7)	0.223	0.218	0.208	0.218
Open Shrubland Australia (7)	0.175	0.174	0.177	0.173
Open Shrubland other (7)	0.132	0.121	0.136	0.140
Woody Savanna (8)	0.118	0.118	0.103	0.122
Savanna (9)	0.138	0.143	0.119	0.133
Grassland (10)	0.188	0.186	0.166	0.184
Cropland Eurasia (12)	0.147	0.153	0.139	0.142
Cropland East Asia, India (12)	0.141	0.141	0.143	0.141
Cropland other (12)	0.153	0.149	0.153	0.155
Barren in Sahara and the Arabian desert (16)	0.368	0.357	0.354	0.367
Barren in Asia (16)	0.230	0.230	0.232	0.229
Barren excluding Sahara, the Arabian desert and Asia (16)	0.178	0.174	0.182	0.178

Table 1: Black sky surface albedo values for various land cover types according to the IGBP vegetation classes given for 4 months as 4 years mean. For February the cropland surface albedo values have been taken as an averaged of the values from May, August, and November.

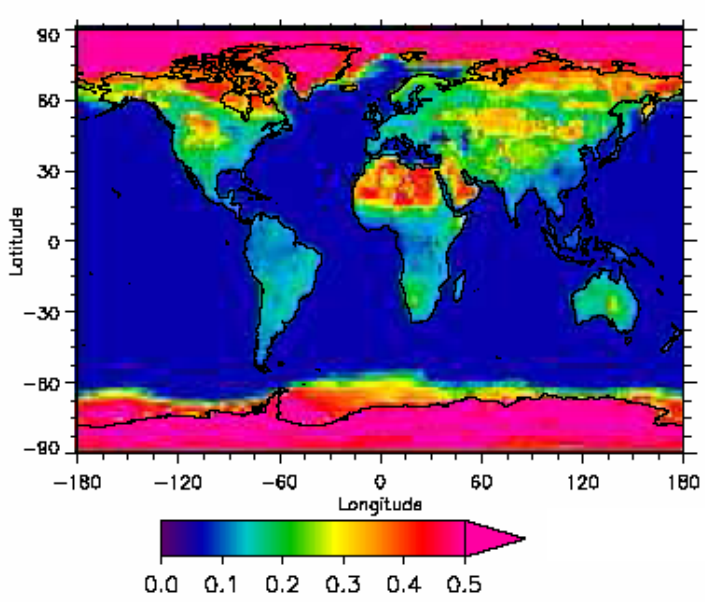

Figure 1: Annual mean surface albedo based on the MODIS black sky and white sky surface albedo

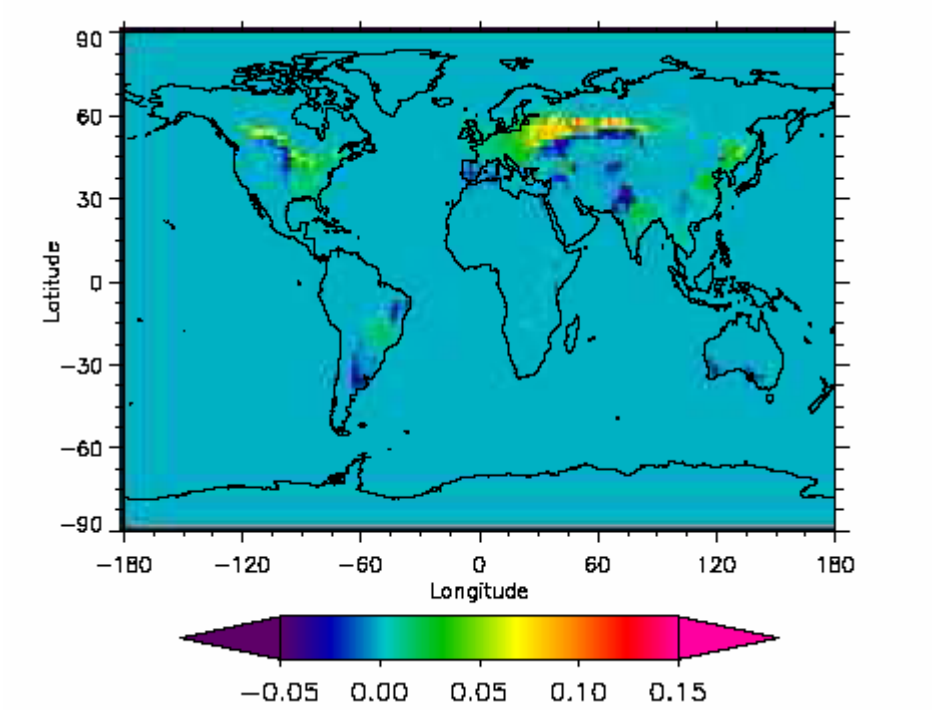

Figure 2: Annual mean surface albedo change caused be vegetation changes

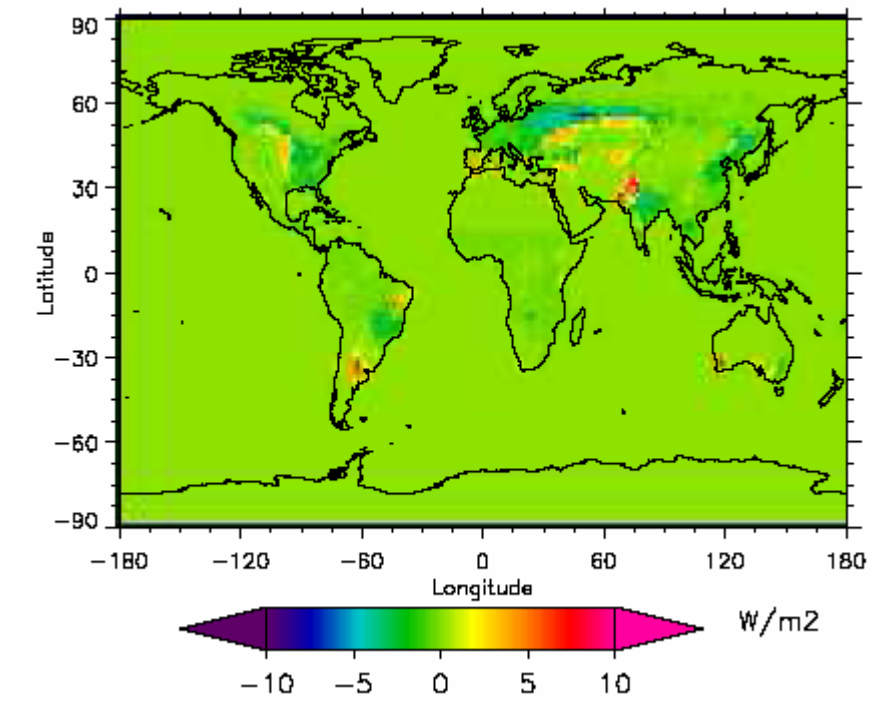

Figure 3: Annual mean radiative forcing due to surface albedo changes caused by vegetation changes.